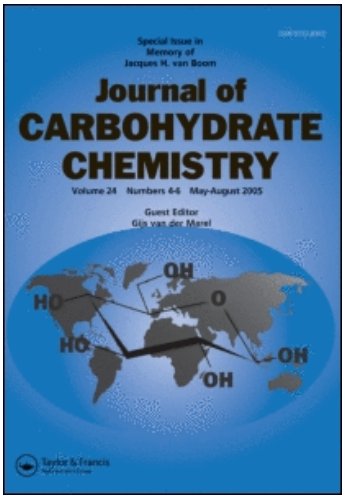

Journal of Carbohydrate Chemistry
Publication details, including instructions for authors and subscription information:
http://www.informaworld.com/smpp/title~content=t713617200

Conformational Analysis of Thiosugars: Theoretical NMR Chemical Shifts and $^{3}J_{H,H}$ Coupling Constants of 5-Thio-Pyranose Monosaccharides

Alonso Aguirre-Valderrama[a]; José A. Dobado[a]
[a] Grupo de Modelización y Diseño Molecular, Departamento de Química Orgánica, Facultad de Ciencias, Universidad de Granada, Granada, Spain

To cite this Article Aguirre-Valderrama, Alonso and Dobado, José A.(2006) 'Conformational Analysis of Thiosugars: Theoretical NMR Chemical Shifts and $^{3}J_{H,H}$ Coupling Constants of 5-Thio-Pyranose Monosaccharides', Journal of Carbohydrate Chemistry, 25: 7, 557 — 594
To link to this Article: DOI: 10.1080/07328300600966471
URL: http://dx.doi.org/10.1080/07328300600966471

Journal of Carbohydrate Chemistry, 25:557–594, 2006

ISSN: 0732-8303 print 1532-2327 online
DOI: 10.1080/07328300600966471

Conformational Analysis of Thiosugars: Theoretical NMR Chemical Shifts and $^3J_{H,H}$ Coupling Constants of 5-Thio-Pyranose Monosaccharides

Alonso Aguirre-Valderrama and José A. Dobado

Grupo de Modelización y Diseño Molecular, Departamento de Química Orgánica, Facultad de Ciencias, Universidad de Granada, Granada, Spain

The conformational space of D and L, deoxy and nondeoxy, 5-thio-pyranoses with biological properties as enzymatic inhibitors was explored using MM and B3LYP/6−31 + G* methods in gas phase and solution. The preferred ring conformation for α and β anomers of 5-thio-L-fucopyranose was the $^1C_4$ form (about 99%), and for 5-thio-D-glucopyranose and 5-thio-D-mannopyranose, the $^4C_1$ one. The experimental conformational order ($^4C_1 > {}^1C_4 > {}^2S_S$) for L-ido derivatives was reproduced only considering the solvent, though for 3-*O*-methyl-5-thio-α-L-idopyranose, the inclusion of methyl in C_3 changed the ^2S_S form to the $B_{1,4}$ one.

Keywords Thiosugars, Thiopyranoses, 5-Thio-sugars, 5-Thiopyranoses, Conformational analysis

INTRODUCTION

Glycosidases are important enzymes that are involved in many diseases and metabolic disorders, such as diabetes, microbial infections, and metastasis.[1] Inhibition of these enzymes is a challenging goal of carbohydrate-based therapy.[2] Saccharides, a source of those natural inhibitors, constitute

Received December 22, 2005; accepted July 4, 2006.
Address correspondence to José A. Dobado, Grupo de Modelización y Diseño Molecular, Departamento de Química Orgánica, Facultad de Ciencias, Universidad de Granada, 18071 Granada, Spain. E-mail: dobado@ugr.es

potential therapeutic agents, but unfortunately are usually degraded in the digestive system and plasma[3,4] by glycosidases, which are abundant in organisms.[5] The use of carbohydrate mimics attempts to solve this problem, being azasugars, in which the ring oxygen is replaced by nitrogen, the most notable.[1,6] However, their nonspecificity is a disadvantage.[7]

In this sense, 5-thio-sugars[7–11] are promising because they resist hydrolysis by glycosidases, as opposed to their homologous natural saccharides. Furthermore, they occasionally show more affinity to receptors than to their natural counterparts.[12] This is the case of 5-thio-α-L-fucopyranose, which is a strong inhibitor of fucosidase due to the increasing hydrophobic interactions between the upper side of the ring and the protein;[7] also, the ring sulphur atom interacts with receptors.[12]

Since the first thiosugar (5-thio-D-xylopyranose) was synthesised in 1961,[13,14] a number of biologically active derivatives have been developed. For instance, 5-thio-glucopyranose[15] inhibits D-glucose transport across cell membranes,[16] cytotoxicity against hypoxic tumor cells,[17] inhibition of plant growth,[18] and other biochemical effects.[8] The 5-thio-D-arabinose[19] and 5-thio-L-galactose[20] compounds have inhibitory activity against α-L-fucosidase from bovine kidney. Deoxythionojirimycin (1-deoxy-5-thio-D-glucose) is a weak inhibitor of α- and β-D-glucosidases,[21] and deoxythiomannojirimycin (1-deoxy-5-thio-D-mannose) is a weak competitive inhibitor or α-D-glucosidase.[22] Thiosugars have been found also in nature as the 5-thio-D-mannopyranose[23] isolated from the marine sponge *Clathria pyramida*[24] or salacinol[25] from *Salacia reticulata*, the herb used in Indian traditional medicine for diabetes, being strong inhibitors of α-glucosidases. On the other hand, unnatural oligosaccharides built up of 5-thio-glycosides have a direct application in the development of oligosaccharide-based drugs such as cancer vaccines[12] and may be used to probe the hydrophobic surface in the binding pocket of oligosaccharide-binding proteins.[7] Nevertheless, to understand these processes all conformational aspects should be considered.

Carbohydrates are multifunctional compounds where the OH groups are used to link different target positions.[26,27] Its experimental characterization is a complex task and, therefore, theoretical information about these 5-thiosugars is critical for a rational design of oligosaccharide-based drugs.[26,28] Moreover, even for a monosaccharide structure, several effects (anomeric,[29] exo-anomeric, (The exo-cyclic O1 lone pair delocalizes into the endocyclic $\sigma^*_{C1—O5}$ bond orbital), hockey-stick (It is defined as the repulsive 1,3 syn-diaxial interaction between the lone pair of an OR (OH in this case) group in axial overlapping with the axial orbital of S_{ring})) determine the conformational distribution.

However, the lack of theoretical studies devoted to thiosugars is evident and, to the best of our knowledge, only one work deals with the greater sweetening power of 5-thio-D-glucose compared to D-glucose[30] and one recent paper reports on the molecular modeling by molecular mechanics (MM) of docked

structures of 5-thio-D-glucopyranosylamine and 5-thio-D-glucopyranosylamidinium bromide in the active site of the protein.[31]

We start this series of theoretical studies exploring the conformational analysis and spectroscopic properties of thiosugars. In the present work, we focus on monosaccharides. Several 5-thio-pyranoses were selected, considering the current trend on the design of small mimic molecules,[32] and the preference for the pyranose form of the free 5-thiosugars in solution.[10] The compounds studied are shown in Scheme 1, 5-thio-α,β-L-fucopyranose (**1** and **2**), 5-thio-α-D-glucopyranose (**3**), 5-thio-α-D-mannopyranose (**4**), and four 5-thio-α-L-idopyranose derivatives (**5**–**8**).[33] The nucleotide of **2** (guanosine 5'-diphospho-5-thio-β-L-fucose), having recently been synthesized, proved to be a substrate for glycosyl transferases valid for the enzymatic syntheses of many valuable oligosaccharides.[12]

In the conformational space of pyranoses, the ring can adopt 38 different canonical forms. Moreover, with only a threefold rotation for each hydroxyl group, the number of possible conformations rises to 38×3^n (where n is the number of hydroxyl groups) for each molecule. Therefore, a key step in the conformational analysis is the choice of an appropriate methodology to explore the potential energy surface. Thus, the conformational search was performed using MM methods in the first stage and extended at the B3LYP/6–31+G* level.

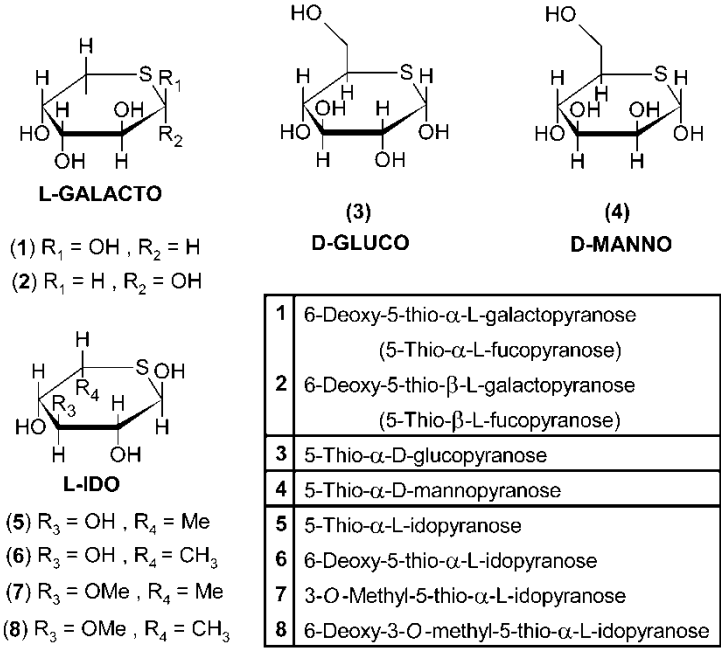

1	6-Deoxy-5-thio-α-L-galactopyranose (5-Thio-α-L-fucopyranose)
2	6-Deoxy-5-thio-β-L-galactopyranose (5-Thio-β-L-fucopyranose)
3	5-Thio-α-D-glucopyranose
4	5-Thio-α-D-mannopyranose
5	5-Thio-α-L-idopyranose
6	6-Deoxy-5-thio-α-L-idopyranose
7	3-*O*-Methyl-5-thio-α-L-idopyranose
8	6-Deoxy-3-*O*-methyl-5-thio-α-L-idopyranose

Scheme 1: 5-Thio-pyranoses under study.

Density functional theory (DFT) methods have been shown to yield results similar to those of MP2.[34,35] Because water is essential in all biological interactions,[36] we also carried out geometrical optimizations with the Polarizable Continuum Model (PCM)[37,38] to account for the solvent effect, and the results were compared with those in the gas phase.

On the other hand, nuclear magnetic resonance (NMR) spectroscopy is a widely used tool for the determination of complex carbohydrate structures.[39,40] Therefore, theoretical calculations of vicinal coupling constants $^3J_{H,H}$ and NMR chemical shifts (δ_H, δ_C) have been performed both in the gas phase and in solution, and compared with the experimental data when available. In addition, the $^3J_{H,H}$ vicinal coupling constants have been calculated using the indirect nuclear spin–spin coupling constants (SSCC)[41,42] method at the B3LYP/6–31+G* level, and computed with the Haasnoot-Leeuw-Altona empirical equation.[43]

COMPUTATIONAL METHODS

Conformational Analysis

In a preliminary step, a conformational search for compounds **1** to **8** was conducted at the MM level using the MMX force field.[44]

To explore the different stable conformers on the whole potential energy surface (PES), we generated 38 canonical ring forms (We used an in-house algorithm to generate the 38 canonical forms (ideal basic conformations) of the pyranose six-membered ring) from a single optimized structure of each molecule (**1**–**8**), and subsequently the corresponding OH rotamers (threefold rotation of 120°) for each ring form. Thus, the total number of structures generated was 3078 (38 ring forms $\times$ 3^4 rotamers) for deoxy molecules and 27,702 (38 ring forms $\times$ 3^6 rotamers) for nondeoxy. After the generation of each individual conformation, the structures were optimized at the MMX force-field method. Thus, a systematic conformational space was explored for all the compounds (**1**–**8**).

Selection of Structures

Due to the computational cost of optimizing at the DFT level all the structures generated for compounds **1**–**8**, it was necessary to develop a systematic approach to select a subset of relevant structures representing the PES. To avoid the automatic discarding of structures of conformational relevance and to explore the PES at DFT level, we used the following strategy: the optimized MMX structures, within a 10 kcal/mol range, were grouped according to its ring form[45] and the rotamers according to the OH dihedral angle values. From each OH group with the same ring form and

dihedral classification, the lowest energy conformation was selected, giving rise to a representative set of rotamers and rejecting numerous duplicated structures in a reliable way.

Two representative sets of rotamers (A and B) were chosen, the A set being up to 5 kcal/mol and the B set from 5 to 10 kcal/mol above the minimum. All the structures from the A set were selected in the final list together with the first rotamers of the B set with the ring form not present in the A set. Although being aware that in an energy range larger than 3 kcal/mol the structures do not contribute meaningfully to the Boltzman populations, we enlarged the cut-off range to 5 kcal/mol for further geometry optimization at B3LYP/6–31G* and B3LYP/6–31+G* levels, with the Gaussian03 program.[46]

Classification of Rotamers by Dihedral Angles

We adopted the common criteria[34,47] of assigning a letter to the dihedral $C_{(i+1)}$-C_i-O-H angle: $g+$ (60°), t (180°) and $g-$ (−60°) (g = gauche; t = anti). Therefore, each letter includes a range for the aforementioned angle, $g+ = 0$ to 120°, $g- = 0$ to −120°, and $t = 120$ to −120°. Thus, each structure is characterized by a sequence of characters (according to the ring-atom numbering) that identifies the OH dihedral (For example, t g+ t g− means OH1 = t, OH2 = g+, OH3 = t and OH4 = g−). In addition to this notation, we also added different arrows (→ and ← to indicate a possible intramolecular hydrogen bonding between contiguous OH groups, (All H···O distances closer to 2.5Å were classified as possible hydrogen bonds) pointing the arrows to the O acceptor atom), as shown in Figures 1 and 2.

Solvent-Effect Calculations

Additional calculations that account for water as a solvent were performed for all the compounds (**1**–**8**) using the default PCM[37,38] in Gaussian03[46] at the B3LYP/6–31+G* level. For this purpose, B3LYP/6–31G* was discarded because the diffuse functions proved necessary for the accurate energy-order reproduction of rotamers and ring forms. Previous calculations using the PM3[48] semiempirical method with the explicit inclusion of the solvent reproduced the interchange of the chair forms of L-ido compounds in solution compared to the gas phase results in the same form as it is discussed in the next section. However, the PM3 method was unable to solve the rotamer analysis, and therefore this method was discarded. We used an implicit solvent model in Gaussian03[46] that allows NMR calculations and geometrical optimizations. The Onsager[49] method failed to reproduce the aforementioned interchange of the chair forms while the PCM

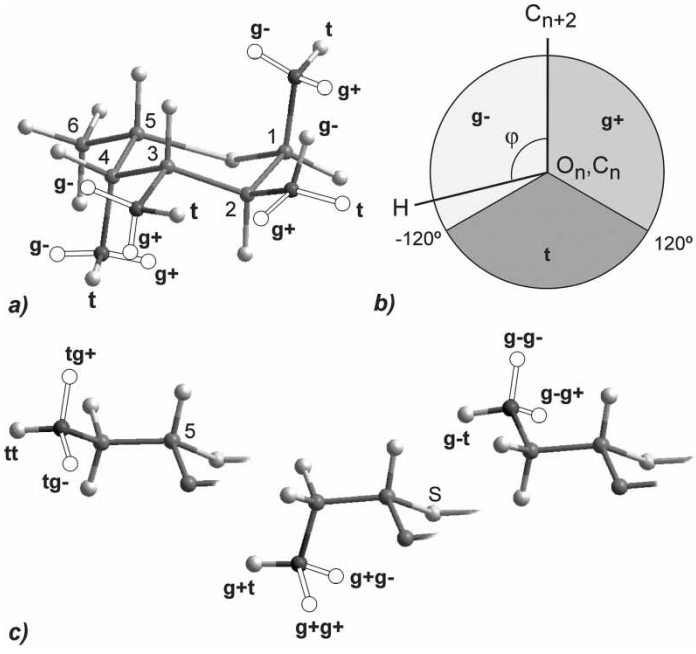

Figure 1: Adopted criterion to assign the dihedral angle of rotamers. (a) The different orientations of the OH dihedrals for the 5-thio-α- L-fucopyranose. (b) Range values for the g+, g-, and t orientations of rotamers. (c) Illustration (only for L-Ido configuration) of the different orientations at C_5 when C_6 presents a CH_2OH group.

method gave good results. Other available methods do not permit geometrical optimizations.

NMR Chemical Shifts and $^3J_{H,H}$ Calculations

The $^3J_{H,H}$ coupling constants were computed using the implementation of indirect nuclear SSCC[41,42] with the Gaussian03[46] program at the B3LYP/6–31+G* level, and also using the Haasnoot-Leeuw-Altona empirical equation,[43] the two methods in the gas phase and in solution, respectively.

The ^{13}C and ^1H NMR chemical shifts were also calculated in the gas phase and in solution with the Gaussian03 program[46] by means of the GIAO method,[50] using tetramethylsilane as a reference ($\delta_C = 190.8$ and $\delta_H = 32.1$ ppm in solution (PCM-B3LYP/6–31 + G*) and $\delta_C = 191.4$ and $\delta_H = 32.0$ ppm in gas phase at the (B3LYP/6–31 + G*)).

For comparisons with the experimental data, the average values of both coupling constants and chemical shifts were computed using the mole fractions—populations—(N_i) given by the Boltzman distribution (Eq. (1)), where g_i is the number of identical conformations of conformer i (statistical weight)

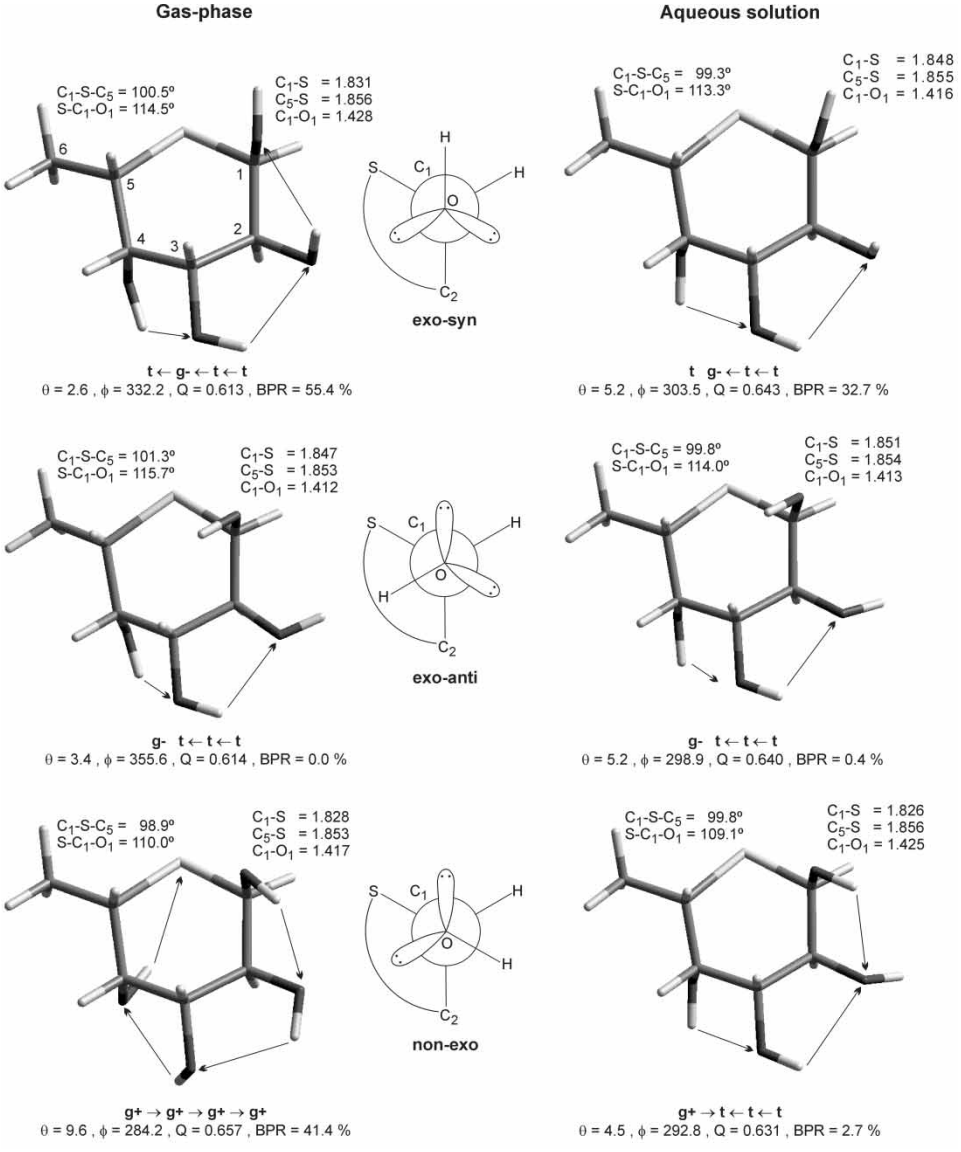

Figure 2: Selected bond distances and angles (Å and degrees) for the most stable rotamers of each possible orientation of the anomeric OH for compound **1** in the gas phase and in solution, and scheme of top view of the C_1-O bond (exo-syn, exo-anti, and non-exo, according to the exo-anomeric effect). Puckering coordinates (θ, ϕ, Q) and Boltzman population rates (BPR) are also included. The arrows indicate OH · · · O interaction between OH groups.

and ΔE_i is the energy of the ith conformer.

$$N_i = \frac{g_i e^{-E_i/RT}}{\sum_i g_i e^{-E_i/RT}} \quad (1)$$

RESULTS AND DISCUSSION

Conformational Analysis

*5-Thio-α-L-fucopyranose **(1)** and 5-Thio-β-L-fucopyranose **(2)***

After completing the structure selection process at the MMX level (see Computational Methods), we obtained a final number of 185 and 238 conformations, within a 10 kcal/mol energy range, for **1** and **2**, respectively. The number of structures resulting from the refining process with B3LYP/6−31+G*, described in the methodological section, was 37 and 31 structures for **1** and **2**, respectively.

Theoretical calculations in the gas phase of the natural counterpart α-L-fucopyranose indicated that the most stable conformation presented maximal intramolecular OH···O interactions.[34,51] This behavior was reproduced only with methods that include electron correlation, and therefore this indicated that the B3LYP/6−31G* level was a valid method for these molecules.[34]

For validation of our conformational analysis procedure, the analysis at B3LYP/6−31G* was extended to the natural counterparts of both the α- and β-anomers, and the results for the α- anomer were compared with the aforementioned previous theoretical works,[34,51] resulting mainly in agreement. In MM methods, the only disagreement appeared for the remaining ring forms, which have a negligible conformational weight.

However, in case of 5-thio-α-L-fucopyranose, these calculations at the B3LYP/6−31G* level failed to describe the exoanomeric effect (The exo-cyclic O1 lone pair delocalizes into the endocyclic σ^*_{C1-O5} bond orbital) due to the presence of stabilizing OH···S_{ring} intramolecular interactions, as it is explained below. Therefore, considering the presence of these long-range interactions, we introduced diffuse functions to the basis set.

For example, the first two rotamers for the natural analog of **1** (α-L-fucopyranose) are [$t \leftarrow g- \leftarrow$ t $\leftarrow t$] and [$g+ \rightarrow g+ \rightarrow g+ \rightarrow g+$] $^1C_4$[34] in concordance with the exo-anomeric effect, which favors the *1t* orientation.[52] These two rotamers have the maximal numbers of OH···O interactions (anticlockwise and clockwise, respectively), which improve their stability.

Sulphur, though less electronegative than oxygen, still induces this exo-anomeric effect in 5-thio-glycosides.[53] However, calculations without diffuse functions inverted the energetic order of the two main contributing conformations. This resulted probably because the 4 $g+$orientation of [$g+ \rightarrow g+ \rightarrow g+ \rightarrow g+$] conformer led to a OH(4)···S_{ring} interaction, which gave additional stabilization.[34] However, the inclusion of diffuse functions (B3LYP/6−31+G*) yielded both rotamers in the same energy order as in the α-L-fucopyranose. Other similar energy-order inversions, depending on the calculation method, were found for **1**.

Also, it is remarkable how the B3LYP/6−31G* level yields overestimated stability to the ring-form alternative to the $^1C_4$ conformation in **2**, in confrontation to the B3LYP/6−31 + G* level. These artificially stabilized ring forms are two $^4C_1$ rotamers, [*g*+ *g*− *g*− → *g*−] and [*g*+ *g*− *g*− → *t*], one $^5S_1$ [*g*+ *g*− *g*+ ← *t*], and one $^4C_1$ [*g*+ *g*− *t* ← *g*+]. The common fact for these alternative ring forms are the *1 g*+ and *2 g*− orientation. The first orientation gives rise to a nonadjacent OH(1) → OH(3) interaction for $^4C_1$ and a double nonadjacent interaction OH(1) → OH(4)/OH(1) ← OH(3) for $^5S_1$. The second orientation induces overestimated stabilizing OH(2)···S_{ring} interaction, presumably caused by the absence of diffuse functions in the basis used.

In contrast to the B3LYP/6−31G* level, the B3LYP/6−31+G* level yields the mentioned $^4C_1$ and $^5S_1$ rotamers at a higher energy, strongly decreasing their population (further calculations at MP2/6−311++G** level for these specific conformers supported this result, as it is shown in Table 6).

On the other hand, the results in the gas phase at B3LYP/6−31+G* of the α- and β- anomers of 5−thio-L-fucopyranose for the main ring form ($^1C_4$) showed the same pattern as its natural analog; that is, the most stable rotamers are those with a maximal number of OH···O interactions, forming intramolecular anticlockwise or clockwise unidirectional chains of hydroxyl groups. Moreover, when these interactions were directed at one oxygen (bidirectional chains, for instance, to C_2 position in the α−$^1C_4$ rotamer [*g*+ → *t* ← *t* ← *t*]), the resulting conformations were less stable.

Tables 1 and 2 list the conformer distribution at the B3LYP/6−31+G* level in the gas phase and in solution for the α- and β-thiofucopyranose. In both cases (α and β), when the solvent was taken into account, the ring forms were automatically classified according to their relative energy, while for calculations in the gas phase the ring forms appear mixed.

From the comparison between the gas phase and solution conformers, the relative energy range was narrower in solution. Thus, for example, the first 10 rotamers of the α-anomer were in a 3.25 kcal/mol energy range in the gas phase and in a 1.67 kcal/mol range in solution, yielding for the β-anomer similar energy ranges of 3.33 and 1.17 kcal/mol, respectively. On the other hand, when the optimization includes the PCM method, some rotamers turn the OH groups to avoid the adjacent OH···O interactions with a much more favorable position for interacting with solvent molecules. For instance, the α-$^1C_4$ [*t* ← g− *g*+ → *g*−] and α-$^1C_4$ [*t* ← *g*− *g*+ → *g*+] rotamers in the gas phase (12th and 5th), after solution, break two of their adjacent OH···O interactions, becoming the second and third most stable rotamers. This stabilization is due to the presence of four and three free OH groups, respectively. The main rotamer for both gas phase and solution [*t* ← *g*− ← *t* ← *t*] / [*t g*− ← *t* ← *t*] also breaks the 1 ← 2 interaction (Figs. 2 and 3) for further stabilization with the solvent. Although the trend is also visible for β-fucopyranose, these breaks are not as evident as in the α-anomer.

Table 1: Comparative Results for 5-Thio-α-L-fucopyranose (**1**) between the gas-phase and aqueous solution at the B3LYP/6–31+G* theoretical level.

	OH rotamers[a]												
Cf[b]	**OH1**		**OH2**		**OH3**		**OH4**	**sring**[c]	**hck**[d]	**free OH**[e]	**exo**[f]	**ΔE**[g]	**BPR**[h]
Gas-phase													
$^{1}C_{4}$	t	←	g−	←	t	←	t		4	1	exs	0.00	55.3
$^{1}C_{4}$	g+	→	g+	→	g+	→	g+	4 → S			nex	0.17	41.4
$^{1}C_{4}$	t		g+	→	g+	→	g+	4 → S		1	exs	2.10	1.6
$^{1}C_{4}$	g+	→	g+	→	g+	→	g−		4	4	nex	2.56	0.7
$^{1}C_{4}$	t	←	g−		g+	→	g+	4 → S		1	exs	3.25	0.2
$^{1}C_{4}$	g+	→	t	←	t	←	t		4	2	nex	3.32	0.2
$^{1}C_{4}$	t	←	g−	←	t		g+	4 → S		1	exs	3.34	0.2
$^{1}C_{4}$	t		t	←	t	←	t		4	1,2	exs	3.41	0.2
$^{1}C_{4}$	g+	→	g+	→	g−	←	t		4	3	nex	3.75	0.1
$^{1}C_{4}$	t		g+	→	g+	→	g−		4	1,4	exs	4.43	0.0
$^{1}C_{4}$	t		g+	→	g−	←	t		4	1,3	exs	4.88	0.0
$^{1}C_{4}$	t	←	g−		g+	→	g−		4	1,4	exs	5.30	0.0
$^{1}C_{4}$	g+	→	t	←	t		g+	4 → S		1,2	nex	5.72	0.0
$^{4}C_{1}$	g−	→	g−		t	←	g+	2 → S		3	exa	6.00	0.0
$^{4}C_{1}$	g−	→	g−		g−	→	t	2 → S		4	exa	6.22	0.0
$^{1}C_{4}$	g−		t	←	t	←	t		4	2	exa[i]	6.31	0.0
$^{1}C_{4}$	g+	→	g+	→	g−		g−		4	3,4	nex	6.82	0.0
$^{1}C_{4}$	t		t	←	t		g+	4 → S		1,2	exs	6.90	0.0
$^{2,5}B$	t	←	t		g+	→	g+	4 → S		1	exs	7.13	0.0
$^{4}C_{1}$	t	←	t		g−	→	t		2	1,4	exs	7.62	0.0
$^{4}C_{1}$	t	←	t		g−	→	g−		2	1,4	exs	7.69	0.0
$^{4}C_{1}$	t	←	t		t	←	g+		2	1,3	exs	7.87	0.0
$^{4}C_{1}$	g−	→	g+		g−	→	g−		2	2,4	exa	8.16	0.0
$^{4}C_{1}$	g−	→	g+		g−	→	t		2	2,4	exa	8.58	0.0

$^{S}S_2$	g−	←	g−	←	t	←	t			1	exa	8.61	0.0
$^{3}S_1$	t	←	t	←	t	←	t		2	1	exs	8.94	0.0
$^{1}C_4$	t		g+	→	g−		g−		4	1,3,4	exs	8.99	0.0
$^{1}S_5$	t	←	g−		g−	→	t			1,4	exs	9.34	0.0
$^{1}C_4$	t		t		g+	→	g−		4	1,2,4	exs	9.44	0.0
$^{5}S_1$	t	←	t		t	←	t		2	1,3	exs	9.55	0.0
$^{S}S_2$	t	←	g−	←	t	←	t			1	exs	9.79	0.0
$^{1}S_5$	t		g+	→	g−	→	t			1,4	exs	9.98	0.0
Aqueous solution													
$^{1}C_4$	t		g−	←	t	←	t		4	1,2	exs	0.00	32.7
$^{1}C_4$	t		g−		g+		g−		4	1,2,3,4	exs	0.54	13.1
$^{1}C_4$	t		g−		g+		g+	4 → S		1,2,3	exs	0.73	9.5
$^{1}C_4$	t		t	←	t	←	t		4	1,2	exs	0.87	7.5
$^{1}C_4$	t		g+	→	g+	→	g+	4 → S		1	exs	0.89	7.3
$^{1}C_4$	t		g−	←	t		g+	4 → S		1,2	exs	0.96	6.5
$^{1}C_4$	t		g+	→	g−	←	t		4	1,3	exs	1.05	5.6
$^{1}C_4$	t		g+	→	g+	→	g−		4	1,4	exs	1.06	5.4
$^{1}C_4$	g+	→	t	←	t	←	t		4	2	nex	1.48	2.7
$^{1}C_4$	g+	→	g+	→	g+	→	g+	4 → S			nex	1.67	2.0
$^{1}C_4$	g+	→	g+	→	g+	→	g−		4	4	nex	1.71	1.8
$^{1}C_4$	g+	→	g+	→	g−	←	t		4	3	nex	1.71	1.8
$^{1}C_4$	t		t	←	t		g+	4 → S		1,2	exs	1.74	1.7
$^{1}C_4$	t		t		g+	→	g−		4	1,2,4	exs	1.99	1.1
$^{1}C_4$	g+	→	t	←	t		g+	4 → S		1,2	nex	2.36	0.6
$^{1}C_4$	g−		t	←	t	←	t		4	2	exa[i]	2.67	0.4
$^{4}C_1$	g−	→	g+		g−	→	g−		2	2,4	exa	4.02	0.0
$^{4}C_1$	t	←	t		g−	→	t		2	1,4	exs	4.08	0.0
$^{4}C_1$	t		t		g−	→	g−		2	1,2,4	exs	4.20	0.0
$^{4}C_1$	g−	→	g+		g−	→	t		2	2,4	exa	4.22	0.0

(*continued*)

Table 1: Continued.

Cf[b]	OH rotamers[a]							sring[c]	hck[d]	free OH[e]	exo[f]	ΔE[g]	BPR[h]
	OH1		OH2		OH3		OH4						
$^4C_1$	g−	→	g−		g−	→	t	2 → S		4	exa	4.22	0.0
$^4C_1$	g−	→	g−		t	←	g+	2 → S		3	exa	4.26	0.0
$^4C_1$	t		t		t	←	g+		2	1,2,3	exs	4.49	0.0
$^1S_5$	t		g−		g−	→	t			1,2,4	exs	5.18	0.0
$^1S_5$	t		g+	→	g−	→	t			1,4	exs	5.87	0.0
$^3S_1$	t	←	t	←	t	←	t		2	1	exs	6.15	0.0
$^5S_1$	t	←	t		t	←	t		2	1,3	exs	6.57	0.0
$^5S_2$	g−	←	g−	←	t	←	t			1?	exa	11.26	0.0
$^5S_2$	t	←	g−	←	t	←	t			1	exs	11.47	0.0

[a]Classification by dihedral angles (see text); the OH groups are numbered according to the ring carbons (see Fig. 1). The arrows indicate OH · · · O interaction between adjacent hydroxyls.
[b]Ring conformation.
[c]Number of ring carbons with an OH · · · S_{ring} interaction.
[d]Number of ring carbons which shows the hockey-stick effect.
[e]Number of ring carbons for which the OH groups are in advantageous orientation to interact with water molecules of solvent.
[f]Exo-anomeric effect being exs = exo-syn, exa = exo-anti, and nex = non-exo.
[g]Relative energy in kcal/mol.
[h]Boltzman population rate.
[i]The exo-anomeric effect is favorable, but this orientation has 1,3 syn-diaxial steric impediment.

Table 2: Comparative results for 5-Thio-β-L-fucopyranose (**2**) between the gas-phase and aqueous solution at the B3LYP/6–31+G* theoretical level.

	OH rotamers[a]													
Cf[b]	**OH1**		**OH2**		**OH3**		**OH4**	**nadj**[c]	**sring**[d]	**hck**[e]	**free OH**[f]	**exo**[g]	**ΔE**[h]	**BPR**[i]
Gas-phase														
$^1C_4$	g−	→	g+	→	g+	→	g+		4 → S		1	nex	0.00	0.40
$^1C_4$	t	←	t	←	t	←	t			4	1	exs	0.16	0.30
$^1C_4$	g+	←	t	←	t	←	t			4	1	exa	0.24	0.27
$^1C_4$	t		g+	→	g+	→	g+		4 → S		1	exs	2.05	0.01
$^1C_4$	t	←	t	←	t		g+		4 → S		1	exs	2.57	0.01
$^1C_4$	t	←	t		g+	→	g+		4 → S		1	exs	2.67	0.00
$^1C_4$	g−	→	g+	→	g+	→	g−			4		nex	3.04	0.00
$^4C_1$	g+		g−		g−	→	t	1 → 3	2 → S		4	exa[j]	3.11	0.00
$^4C_1$	g+		g−		g−	→	g−	1 → 3	2 → S		4	exa[j]	3.14	0.00
$^1C_4$	g+	←	t	←	t		g+		4 → S		1	exa	3.33	0.00
$^1C_4$	g+	←	t		g+	→	g+		4 → S		1	exa	3.67	0.00
$^4C_1$	g+		g−		t	←	g+	1 → 3	2 → S		3	exa[j]	3.79	0.00
$B_{1,4}$	g+		g−		t	←	t	1 → 4	2 → S		3	exa[j]	3.81	0.00
$^1C_4$	g−	→	g+	→	g−	←	t			4	3	nex	4.21	0.00
$^5S_1$	g+		g−		g+	←	t	1 → 4, 1 ← 3	2 → S			exa[j]	4.22	0.00
$^1C_4$	g+		g+	→	g+	→	g−			4	1,4	exa	4.37	0.00
$^3S_1$	g+		t	←	t	←	t	1 → 4			2	exa[j]	4.63	0.00
$^5S_1$	t		g+		g+	→	g+	1 ← 4		2	1,2	exs	5.08	0.00
$^5S_2$	t	←	t	←	t		t				1,2	exs	5.28	0.00
$^1C_4$	t		g+	→	g+	→	g−			4	1,4	exs	5.33	0.00
$^{2,5}B$	g+		t		g−	→	g+	2 ← 5, 1 → 3	4 → S		1	exa	5.41	0.00

(*continued*)

Table 2: Continued.

Cf[b]	OH rotamers[a]							nadj[c]	sring[d]	hck[e]	free OH[f]	exo[g]	ΔE^h	BPR[i]
	OH1		OH2		OH3		OH4							
$^1C_4$	g+		g+	→	g−	←	t			4	1,3	exa	5.51	0.00
$^4C_1$	g+		t		g−	→	t	1 → 3		2	2,4	exa[j]	5.67	0.00
$^1C_4$	t	←	t		g+	→	g−			4	1,4	exs	5.73	0.00
$^1C_4$	g+	←	t		g+	→	g−			4	1,4	exa	5.84	0.00
$^5S_1$	g+		g+		g+	←	t	1 ← 3, 1 → 4		2	2	exa[j]	6.02	0.00
$^1C_4$	t		g+	→	g−	←	t			4	1,3	exs	6.34	0.00
$^1S_5$	t	←	t	←	t	←	g+				1	exs	6.39	0.00
$^4C_1$	g+		g+		g−	→	g−	1 → 3		2	2,4	exa[j]	6.50	0.00
^2S_S	g+		t		g−	→	t	1 → 3			2,4	exa[j]	7.82	0.00
$^1S_5$	t	←	t		g−	→	t				1,4	exs	9.99	0.00
Aqueous solution														
$^1C_4$	g+	←	t	←	t	←	t			4	1	exa	0.00	0.25
$^1C_4$	t	←	t	←	t	←	t			4	1	exs	0.06	0.23
$^1C_4$	t	←	t	←	t		g+		4 → S		1	exs	0.70	0.08
$^1C_4$	g+	←	t	←	t		g+		4 → S		1	exa	0.78	0.07
$^1C_4$	t	←	t		g+	→	g+		4 → S		1	exs	0.79	0.07
$^1C_4$	g+	←	t		g+		g+		4 → S		1,3	exa	0.96	0.05
$^1C_4$	g+	←	t		g+		g−			4	1,3,4	exa	1.08	0.04
$^1C_4$	g+		g+	→	g+	→	g−			4	1,4	exa	1.09	0.04
$^1C_4$	t	←	t		g+	→	g−			4	1,4	exs	1.11	0.04
$^1C_4$	t		g+	→	g+	→	g+		4 → S		1	exs	1.17	0.04
$^1C_4$	g+		g+	→	g−	←	t			4	1,3	exa	1.19	0.03

$^1C_4$	t		g+	→	g+	→	g−			4	1,4	exs	1.44	0.02
$^1C_4$	t		g+	→	g−	←	t				1,3	exs	1.59	0.02
$^1C_4$	g−		g+	→	g+	→	g+		4 → S		1	nex	1.73	0.01
$^1C_4$	g−		g+	→	g+	→	g−			4	1	nex	1.88	0.01
$^1C_4$	g−	→	g+	→	g−	←	t			4	3	nex	2.02	0.01
$^3S_1$	g+		t	←	t	←	t	1 → 4			2	exa[j]	3.49	0.00
$^4C_1$	g+		g−		t	←	g+	1 → 3	2 → S		3	exa[j]	4.56	0.00
$^4C_1$	g+		t		g−	→	t	1 → 3		2	2,4	exa[j]	4.68	0.00
$^4C_1$	g+		g−		g−	→	g−	1 → 3	2 → S		4	exa[j]	4.71	0.00
$^4C_1$	g+		g+		g−	→	g−	1 → 3		2	2,4	exa[j]	4.79	0.00
$^4C_1$	g+		g−		g−	→	t	1 → 3	2 → S		4	exa[j]	4.83	0.00
$B_{1,4}$	g+		g−		t	←	t	1 → 4	2 → S		3	exa[j]	5.05	0.00
$^5S_1$	t		g+		g+	→	g+	1 ← 4		2	1	exs	5.49	0.00
$^1S_5$	t	←	t	←	t	←	g+				1	exs	5.71	0.00
$^5S_1$	g+		g+		g+	←	t	1 ← 3, 1 → 4		2	2	exa[j]	5.82	0.00
$^1S_5$	t	←	t		g−	→	t				1,4	exs	5.86	0.00
$^5S_2$	t	←	t	←	t		t				1,2	exs	7.42	0.00
$^2S_5$	g+		t		g−	→	t	1 → 3			2,4	exa[j]	8.64	0.00

[a]Classification by dihedral angles (see text); the OH groups are numbered according to the ring carbons (see Fig. 1). The arrows indicate OH · · · O interaction between adjacent hydroxyl.
[b]Ring conformation.
[c]OH. . .OH interactions between nonadjacent OH groups, the number indicating the ring carbon.
[d]Number of ring carbons with an OH · · · S_{ring} interaction.
[e]Number of ring carbons, which show the hockey-stick effect.
[f]Number of ring carbons for which the OH groups are in advantageous orientation to interact with water molecules of solvent.
[g]Exo-anomeric effect being exs = exo-syn, exa = exo-anti, and nex = non-exo.
[h]Relative energy in kcal/mol.
[i]Boltzman population rate.
[j]The OH group is endo but is stabilized by the nonadjacent OH · · · OH interaction.

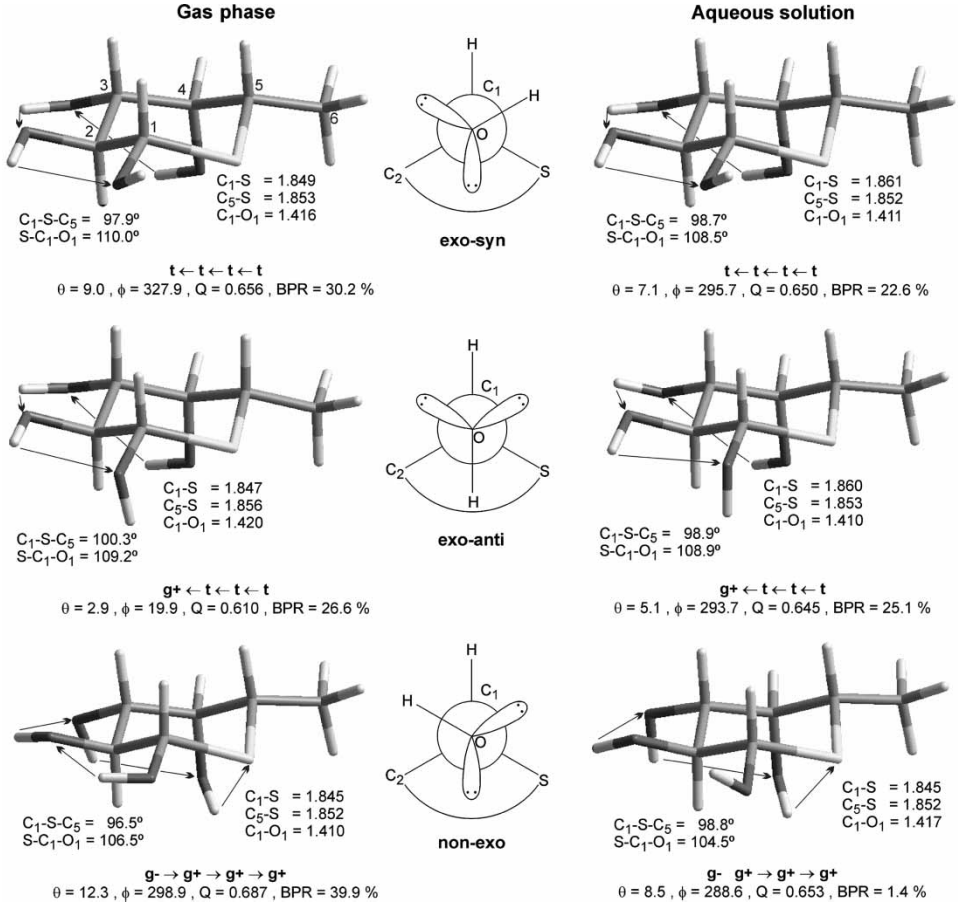

Figure 3: Selected bond distances and angles (Å and degrees) for the most stable rotamers of each possible orientation of the anomeric OH for compound **2** in the gas phase and in solution, and scheme of top view of the C_1-O bond (exo-syn, exo-anti, and non-exo, according to the exo-anomeric effect). Puckering coordinates (θ, ϕ, Q) and Boltzman population rates (BPR) are also included. The arrows indicate OH · · · O interaction between OH groups.

The most remarkable result concerns the exo-anomeric effect. For the $^1C_4$ ring forms of both α- and β-anomers, we find that calculations in solution favorably reproduced the exo-anomeric effect, and the different rotamers are ordered (exo-syn > non-exo > exo-anti for the α, and exo-syn = exo-anti > non-exo for the β) according to this effect (see Tables 1 and 2). Thus, for α-thiofucose, most of the forms with the *1t* orientation, which allows the favorable exo-syn one, are the most stable rotamers, with the exception of [$t\ t \leftarrow t\ g+$] and [$t\ t\ g+ \rightarrow g-$] ones. The non-exo rotamers (*1* $g+$ orientation) are closely grouped above those exo-syn, with a relative energy greater than 1.48 kcal/mol. The exo-anti, which shows 1,3-syndiaxial repulsion of OH(1) with H(3) and H(5), is the less stable

$^1C_4$ rotamer. However, in the gas phase the non-exo rotamers are stabilized and mixed with the exo-syn ones, the relative destabilization of the rotamer [$g+ \rightarrow g+ \rightarrow g+ \rightarrow g+$] from the gas phase (2nd) to solution (10ths) being the most significant, in agreement with the exo-anomeric effect.

For the β-thiofucopyranose (**2**) also the exo-anomeric effect is best reproduced when the solvation effects are included. For $^1C_4$ ring forms, the non-exo conformers are the less stable in the conformational distribution list. Thus, the [$g- \rightarrow g+ \rightarrow g+ \rightarrow g+$] rotamer, which is the most populated one for the gas-phase calculations, becomes the 14th in solution. A similar but less pronounced behavior was noted for the [$g- \rightarrow g+ \rightarrow g+ \rightarrow g-$] rotamer. Now, for the β-anomers, none of the exo forms (exo-syn and exo-anti) have steric interactions and therefore both are equally probable (see Table 2).

The aforementioned trend for breaking the OH···O interactions in solution is less noticeable here. For β-anomers, the first and second most populated rotamers in solution showed the maximum number of OH···O interactions in a unidirectional anticlockwise pattern, a feature that was kept from the corresponding conformers in the gas phase. Nevertheless, the effect of being solvated is still noticed in a slight rotation of OH groups in order to be more accessible to the solvent molecules.

From these results, it can be concluded that calculations in solution result in breaking the intramolecular OH···O interactions, because of the stabilization with the solvent. For both α- and β-anomers in solution, the $^1C_4$ ring forms are the main rotamers. Calculations in the gas phase lead to those ring forms with indifferently clockwise or anticlockwise unidirectional intramolecular OH···O patterns to be the most stable structures. In solution, however, the clockwise forms are energetically penalized, in agreement with the exo-anomeric effect, thus concluding that the gas-phase calculations are unable to reproduce this effect.

*5-Thio-α-D-glucopyranose (**3**) and 5-Thio-α-D-mannopyranose (**4**)*

The CH_2OH group at C_6, present in **3** and **4**, caused a higher amount of rotamers. For both molecules, the situation was similar to that in **1** and **2**, in the sense that, in solution, the different ring forms appeared energetically ordered, and the most contributing conformations lay in a narrower energy range.

Figure 4 shows the most contributing rotamer for **3** and **4** in the gas phase and in solution. Both showed the same pattern as in **1** and **2**, that is, a maximal number of anticlockwise OH···O interactions between adjacent OH groups. Additionally, in the gas phase, the OH group from the hydroxymethyl group participates in the interaction chain in the same direction, but this interaction is eliminated after solution through a change in the rotations of the CH_2OH group. For **3**, as in **1** and **2**, clockwise interaction patterns, after solution, are relatively destabilized, with larger ΔE values. This is again explained with the exoanomeric effect, because these clockwise patterns coincide with

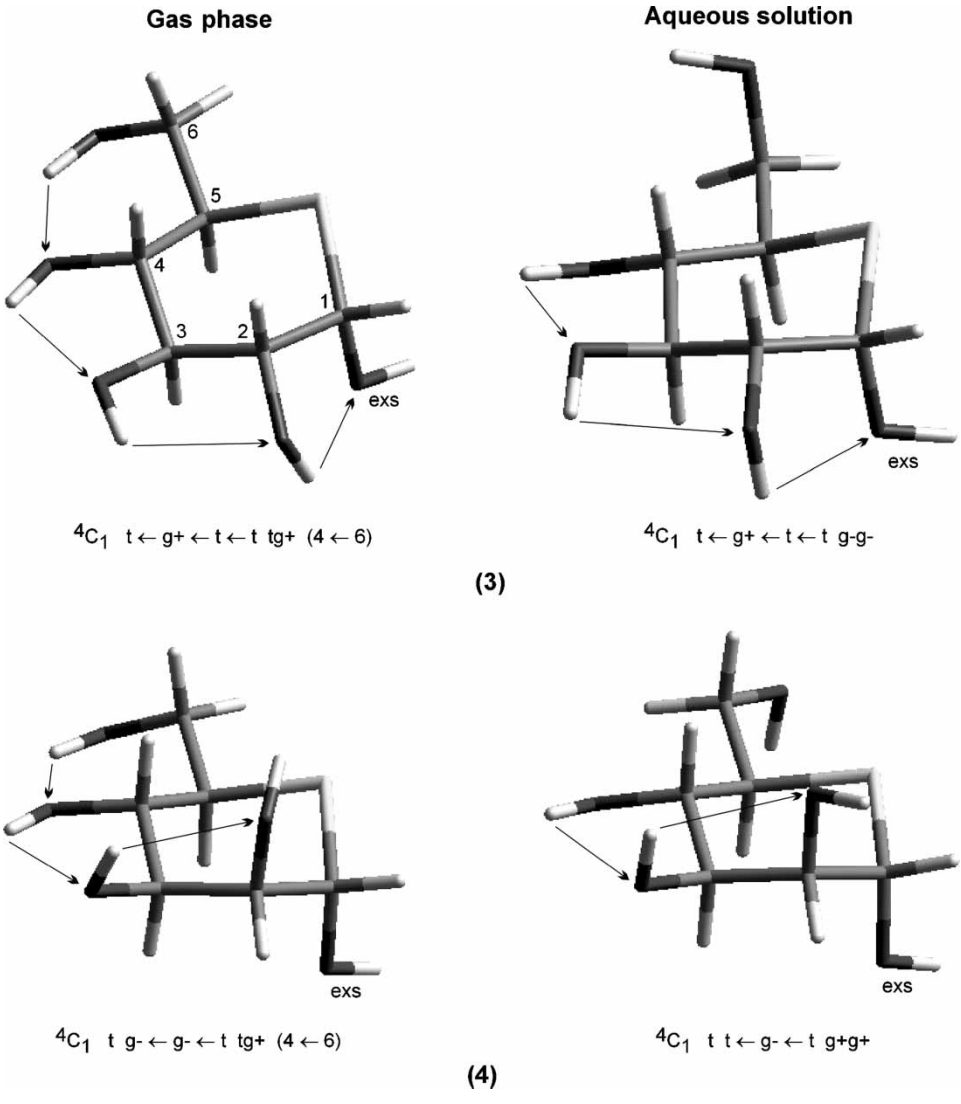

Figure 4: The main rotamers for compounds **3** and **4** in the gas phase and in solution. The orientations of the anomeric OH according to the exo-anomeric effect are depicted (exs: exo-syn). The arrows indicate OH · · · O interaction between OH groups.

non-exo forms for **3**. However, for **4** this effect is not noticeable, due to the impossibility of a OH(1)···OH(2) interaction that could stabilize the non-exo orientation (*1 g-* for **4**), as was the case for **1**–**3**.

*L-Ido derivatives (**5**–**8**)*

Four different L-ido derivatives were studied here, the 5-thio-α-L-idopyranose (**5**), its 6-deoxy compound (**6**), the 3-OMe derivative of **5** (**7**), and its 6-deoxy

compound (**8**). Previous experimental NMR analysis[20,54] concluded the conformational preference of **5** (and some of its derivatives also) to be $^4C_1 > {}^1C_4 > {}^2S_S$. Our current theoretical results in solution were in agreement for **5**, **6**, and **8**, whereas for **7**, the ^2S_S skew-boat was replaced with the $B_{1,4}$ boat in the conformational preference.

The geometries of the first rotamers for each ring form are depicted in Figures 5 to 8. The conformational analysis for deoxy molecules (both in the gas phase and in solution) reproduced the experimental energy order, $^4C_1 > {}^1C_4 > {}^2S_S$, although in the gas phase the $^1C_4$ form was overestimated, as indicated by the experimental $^3J_{H,H}$ data. However, for the nondeoxy structures **5** and **7**, the conformational preferences of the chair rings were interchanged in the gas phase ($^1C_4 > {}^4C_1$), whereas calculations in solution reproduced the experimental energy order ($^4C_1 > {}^1C_4$). Moreover, in solution, the ^2S_S form of **5**, **6**, and **8** ($B_{1,4}$ for **7**) increased their conformational weight.

The rotamer analysis showed remarkable results regarding the favoring of the $^1C_4$ form in the gas phase. For compounds **5**–**8**, the $^1C_4$ form (where OH···O adjacent interactions are not possible) exhibits two nonadjacent hydrogen bonds between OH(1) and OH(3) (OMe for **7** and **8**) and between OH(2) and OH(4). These interactions are responsible for its greater population rates in the gas phase. Furthermore, the nondeoxy molecules present an additional stabilization due to the hydrogen bond between OH(4) and OH(6), thus inverting the conformational preference and favoring this ring form.

On the other hand, taking into account the fact that the adjacent interactions are weaker than nonadjacent ones,[55] the $^4C_1$ form is relatively destabilized with respect to the $^1C_4$ form in the gas phase. Furthermore, the presence of weak unidirectional chain interactions allows, after solution, better interaction with the solvent molecules through the loss of some of these interactions, or reorientation of the OH groups. Furthermore, for the OH(6) group of nondeoxy molecules (**5** and **7**), the free form is preferred instead of its participation in the intramolecular hydrogen bonds, incrementing their relative stability in solution.

The experimental conformational order for 5-thio-L-derivatives (including **5**–**8**) is generally explained in terms of the "hockey-stick" effect. According to this effect, the $^1C_4$ form (with a double effect at C_2 and C_4) should be less stable than the $^4C_1$ ring form. Our results confirm this effect in solution, but not in the gas phase, although, in principle, the "hockey-stick" effect should be valid also for the gas phase. Even more, from our conformational study, several ring forms compatible with this effect were stabilized by intramolecular OH···O interactions, while in other conformers, the rotation of some OH groups gave rise to stabilizing OH···S_{ring} interactions, these being incompatible with the nature of the "hockey-stick" effect.

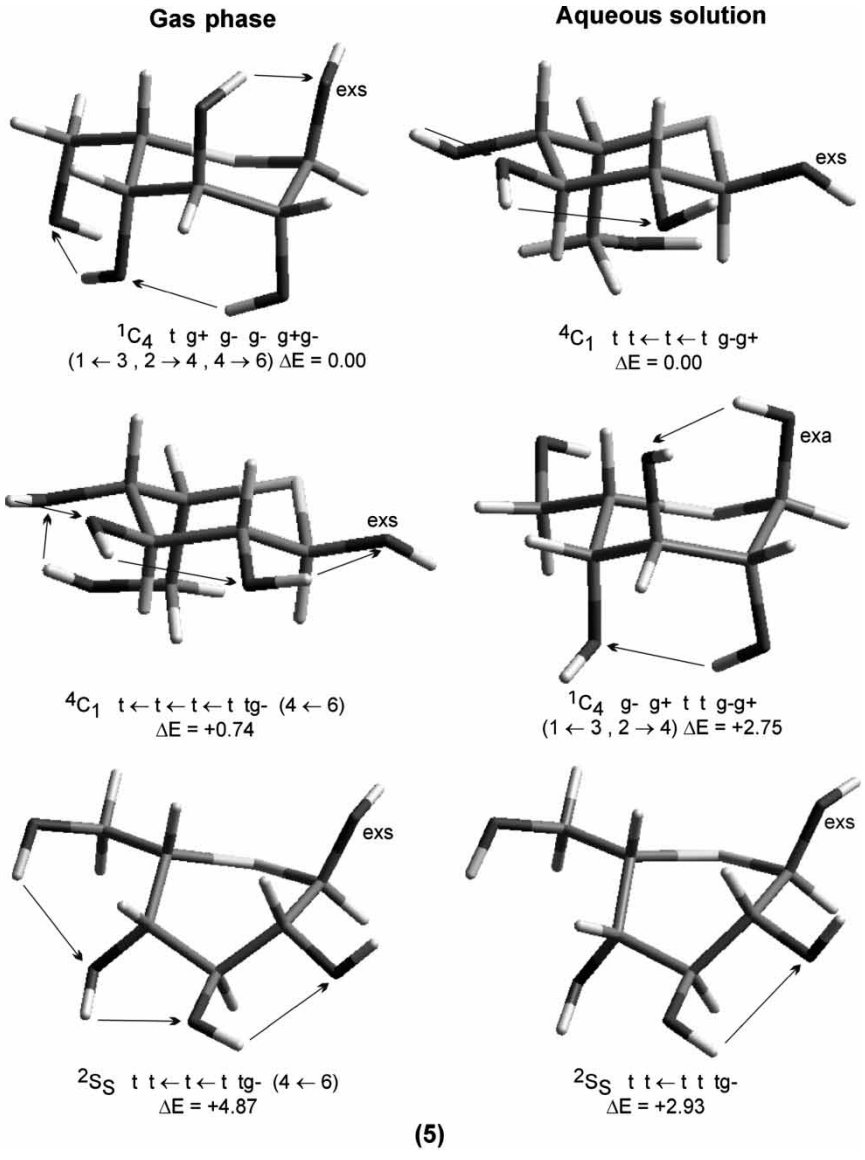

Figure 5: The main rotamers of the most significant conformations for compound **5** in the gas phase and in solution. The orientations of the anomeric OH according to the exo-anomeric effect are depicted (exs: exo-syn, exa: exo-anti). The arrows indicate OH···O interaction between OH groups (the interaction between no adjacent OH groups are noted in parentheses).

All of this indicates that, although valid, the "hockey-stick" effect may not be the determining factor for resolving the conformation in these kinds of molecules, and further studies about the relevance of this effect are necessary.

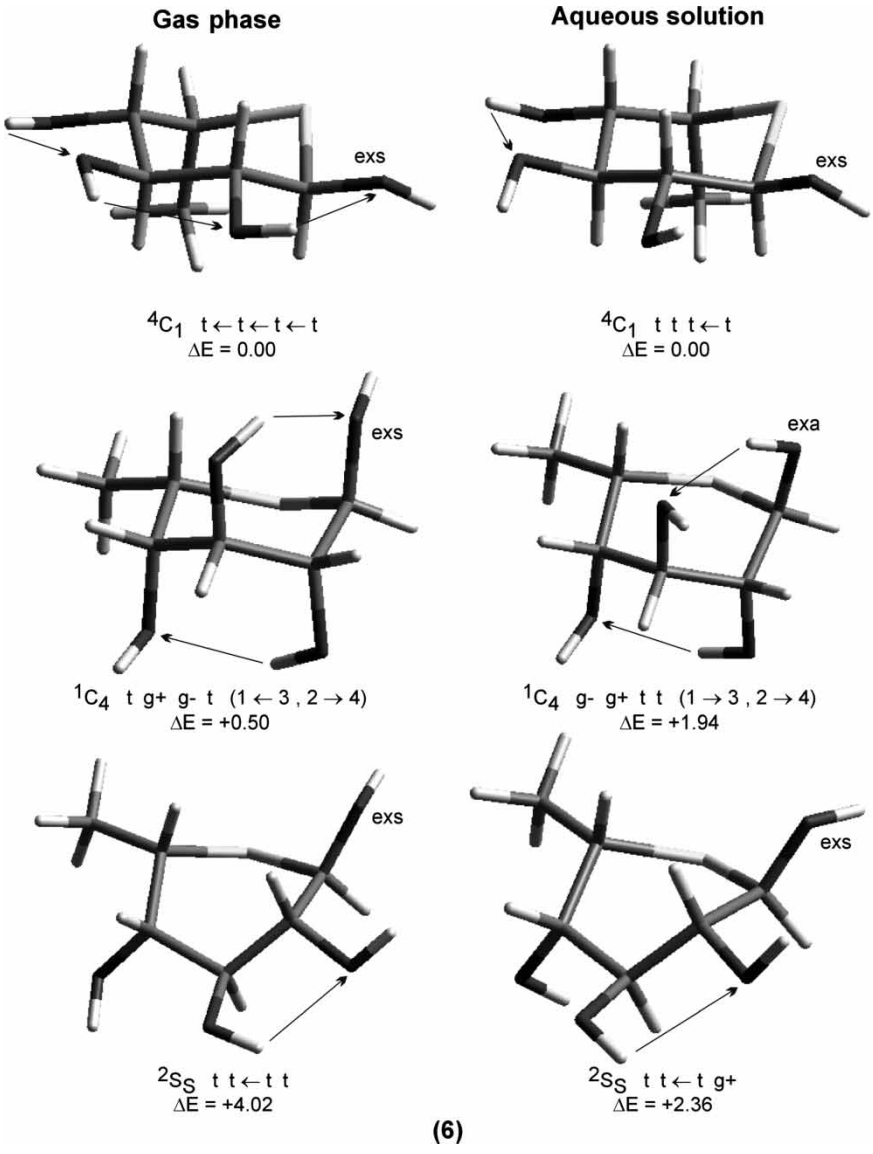

Figure 6: The main rotamers of the most significant conformations for compound **6** in the gas phase and in solution. The orientations of the anomeric OH according to the exo-anomeric effect are depicted (exs: exo-syn, exa: exo-anti). The arrows indicate OH···O interaction between OH groups (the interaction between no adjacent OH groups are noted in parentheses).

Geometrical Parameters

Figures 2 and 3 display a selection of geometric parameters for the most stable structures of **1** and **2**, respectively, such the bond distances, angles, and puckering parameters for each possible exo-anomeric orientation.[5]

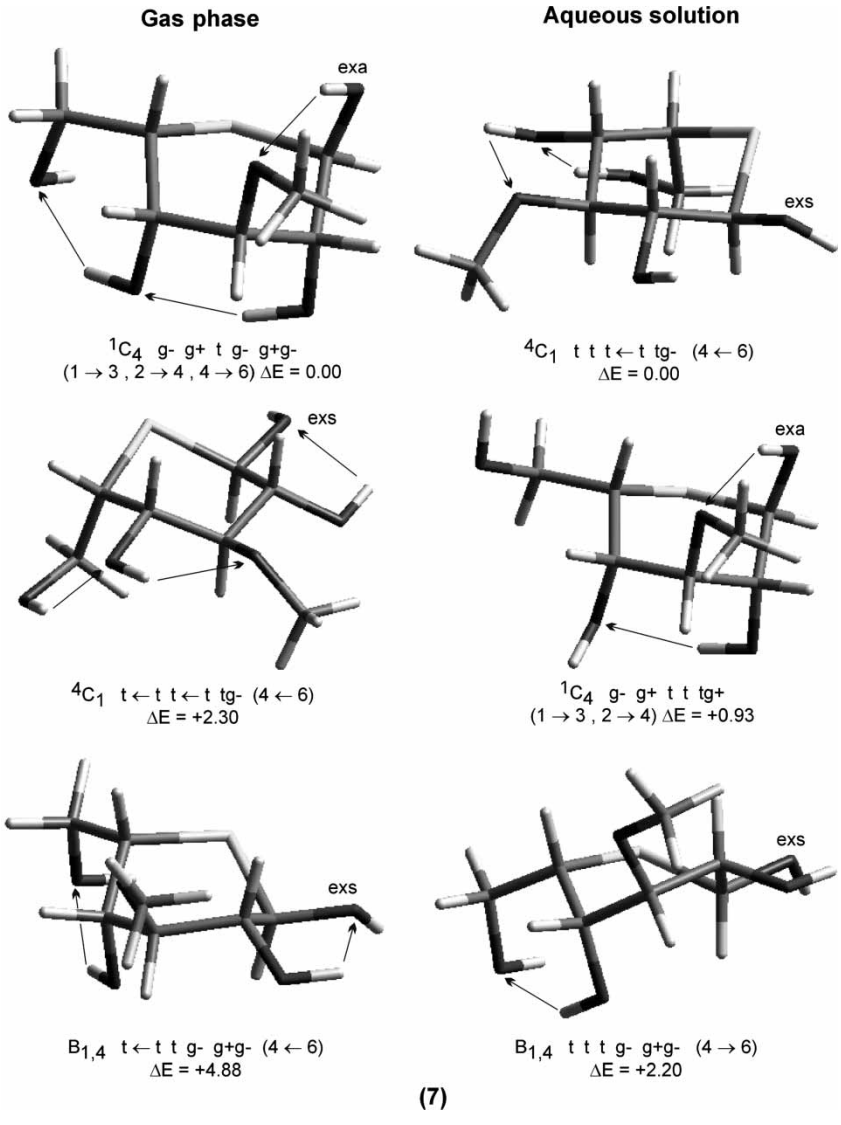

Figure 7: The main rotamers of the most significant conformations for compound **7** in the gas phase and in solution. The orientations of the anomeric OH according to the exo-anomeric effect are depicted (exs: exo-syn, exa: exo-anti). The arrows indicate OH···O interaction between OH groups (the interaction between no adjacent OH groups are noted in parentheses).

Puckering coordinates[45] were used to analyze and classify the resulting ring conformations. As expected, the thiofucose rings showed larger Q values than did fucose, signifying their higher deviation from planarity. On the other hand, $^1C_4$ rings of thiofucose showed a greater twisting than in fucose, indicated by larger θ values. This was also observed in the experimental data

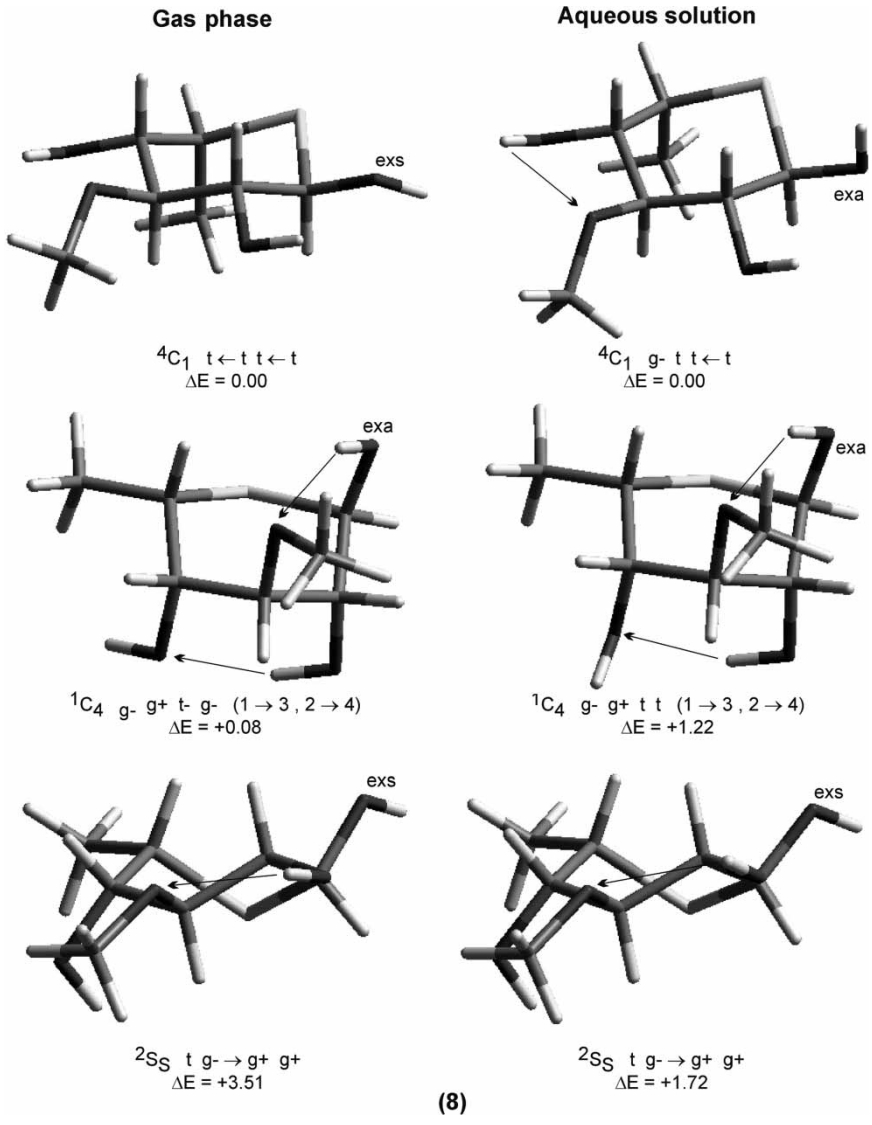

Figure 8: The main rotamers of the most significant conformations for compound **8** in the gas phase and in solution. The orientations of the anomeric OH according to the exo-anomeric effect are depicted (exs: exo-syn, exa: exo-anti). The arrows indicate OH···O interaction between OH groups (the interaction between no adjacent OH groups are noted in parentheses).

for other thiosugars[7,9] and explained with the larger C-S_{ring} bond distance (compared to C-O_{ring}) and the smaller $\angle C_1$-S_{ring}-C_5 angles.

Moreover, our results of fucopyranose agreed well with the X-ray experimental data. Although X-ray and theoretical geometries cannot be directly compared due to the different environments, their comparison can provide

valuable information on the main geometrical trends of the compounds under study and the accuracy of the calculations. The maximal deviations from experimental bond lengths in α-fucopyranose were of 0.034 Å for C_5-O_{ring} and 0.046 Å for C_1-O_1. The remaining distances were in good agreement, including the C_1-O_{ring} distance (deviation of 0.01 Å). However, the bond angles displayed larger deviations of 4.5° and 7.1° for $\angle C_1$-O_{ring}-H and $\angle O_1$-C_1-H_1, respectively. In general, the B3LYP/6−31 + G* method agreed well with the experimental data,[56] supporting this as a correct method for reproduction of pyranose geometries.

Focusing on the studied 5-thiofucopyranoses **1** and **2**, some noteworthy features were examined from a geometrical comparison between these α- and β- anomers. The B3LYP/6−31 + G* geometries, both in the gas phase and in solution, reproduced correctly the anomeric effect.[29] Thus, the C_1-S distance of α-thiofucopyranose was shortened with respect to the β-analog (average values of 1.830 Å vs. 1.836 Å in the gas phase, and 1.845 Å vs. 1.858 Å in solution) whereas the C_1-O_1 distances were lengthened (1.423 Å vs. 1.406 Å and 1.412 Å vs. 1.408 Å). On the other hand, the $\angle$ S-C_1-O_1 angle was lengthened for **1** (in the gas phase 112.6 vs. 107.7° and in solution 112.5 vs. 108.3°). This was expected from the experimental data of monosaccharides[57] and was reproduced correctly, corroborating the presence of the anomeric effect in thiopyranoses.

The exo-anomeric effect in thiosugars was also experimentally evidenced.[5] The most remarkable geometrical results were found for this effect. In opposition to the anomeric one, the exo-anomeric effect for saccharides shortens the C_1-O_1 bond distance and lengths the C_1-O_{ring} one.[57] Our geometric results also indicate that calculations in solution are necessary for reproducing the exo-anomeric effect.

Table 3 lists the C_1-O_1 and C_1-S_{ring} bond-length differences in exo-anomeric forms with respect to the non−exo-anomeric bond lengths, for both the gas phase and in solution. For all compounds studied, results in solution indicate a decreasing length for C_1-O_1 bonds and an increasing one for C_1-S_{ring} bonds, in complete agreement with the overall behavior in monosaccharides. However, gas-phase results generally failed to reproduce the C_1-O_1 bond shortening, resulting in an increase. Additionally, there was a slight agreement in the case of the lengthening of C_1-S_{ring} bond, although bond length increases were occasionally very small.

Finally, in order to allow a direct correlation between the spectroscopic and geometric data, Table 4 summarizes the main calculated structural data in solution for the most stable rotamers of each compound. It is noteworthy that the S-C_1-O_1 angle allows a direct determination of the nature (axial/equatorial) of the anomeric C_1-O_1 bond. Values about 113° and 108° correspond to axial and equatorial arrangements, respectively. Complementarily, this permits to identify the axial/equatorial arrangements for skew boat conformations (e.g., the ^2S_s conformation), where the visual determination is complex.

Table 3: Theoretical exonameric lengthening of C_1-S distance and shortening of C_1-O_1 one, with respect to the corresponding non-exo values (in Å).

			Gas phase		Aqueous solution	
	Cf[a]	**exo**[b]	**Δ C_1-S**	**Δ C_1-O_1**	**Δ C_1-S**	**Δ C_1-O_1**
1	$^1C_4$	exa	+0.019	−0.005	+0.025	−0.012
		exs	+0.003	+0.011	+0.022	−0.009
2	$^1C_4$	exa	+0.002	+0.010	+0.015	−0.007
		exs	+0.004	+0.006	+0.016	−0.006
3	$^4C_1$	exa	+0.027	−0.008	+0.029	−0.013
		exs	+0.013	+0.007	+0.026	−0.011
5	$^4C_1$	exa	+0.005	+0.006	+0.018	−0.009
		exs	+0.008	+0.004	+0.018	−0.008
	$^1C_4$	exa	+0.038	−0.037	+0.028	−0.021
		exs	+0.016	−0.013	+0.016	−0.014
6	$^4C_1$	exa	+0.008	+0.006	+0.017	−0.009
		exs	+0.012	+0.004	+0.019	−0.009
	$^1C_4$	exa	+0.031	−0.036	+0.028	−0.021
		exs	+0.012	−0.011	+0.018	−0.015
8	$^4C_1$	exa	+0.006	+0.007	+0.017	−0.009
		exs	+0.009	+0.005	+0.018	−0.008

[a]Ring conformation.
[b]Exo-anomeric effect being exs = exo-syn and exa = exo-anti.

Spectroscopic Properties

The ^{13}C and ^1H NMR chemical shifts were calculated using the GIAO method in the gas phase and in solution, and the results are graphically displayed in Figure 9 and listed in Table 5.

The main differences between **1** and **2** and their natural counterparts in the gas phase were found for δ_{C1} and δ_{C5} chemical shifts, with a downfield displacement for these thiosugars, and displacements of 15 and 24 ppm, respectively, in the α-anomers (17 and 27 ppm in the case of β-anomers). These values reproduce the experimental trend.[33,58]

Similar results were found for the ^1H shifts when comparing thiosugars **1** and **2** and the fucopyranoses, the δ_{H5} and δ_{H1} values both being downshifted 0.5 ppm for the α-anomer. However, although similar displacements were noted for the δ_{H5} values for the β-anomer (about 0.5 ppm), a small blueshift of about 0.2 ppm was found for δ_{H1}. This effect of the δ_{H1} was found both experimentally and theoretically.[33,58]

For α-anomer of thiofucose **1**, the calculated ^{13}C and ^1H NMR data in the gas phase yielded a better agreement with the experimental data than in solution, the latter δ_{C1} and δ_{C5} being the most deviated chemical shifts. Similar results for the β-anomer **2** were found in the ^1H spectrum. The absence of ^{13}C experimental data for **2** hampers its comparison. In general, the results from calculations in solution yielded higher values than in the

Table 4: Selected geometrical parameters (Å and degrees) and puckering coordinates of compounds **1**–**8** at the B3LYP/6–31+G* theoretical level in solution for the first rotamers of the main ring forms.

		Puckering coordinates							
	Cf[a]	θ	ϕ	**Q**	**C_1-S**	**C_5-S**	**C_1-O_1**	**C_1-S-C_5**	**S-C_1-O_1**
1	$^1C_4$	5.2	303.5	0.643	1.848	1.855	1.416	99.3	113.3
2	$^1C_4$	5.1	293.7	0.645	1.860	1.853	1.410	98.9	108.9
3	$^4C_1$	171.0	112.2	0.661	1.848	1.848	1.413	98.9	113.7
4	$^4C_1$	176.7	105.2	0.621	1.845	1.849	1.416	100.6	113.4
5	$^4C_1$	171.7	117.6	0.645	1.866	1.845	1.409	99.9	107.9
	$^1C_4$	5.6	302.0	0.633	1.858	1.854	1.414	99.6	113.6
	^2S_S	85.2	269.5	0.886	1.863	1.850	1.414	98.2	113.3
6	$^4C_1$	171.0	108.7	0.653	1.864	1.848	1.411	99.7	108.1
	$^1C_4$	5.2	297.9	0.631	1.856	1.856	1.416	99.9	113.4
	^2S_S	85.4	266.9	0.878	1.860	1.851	1.417	98.7	113.2
7	$^4C_1$	173.4	138.6	0.639	1.864	1.842	1.409	100.6	107.5
	$^1C_4$	6.3	294.8	0.638	1.857	1.854	1.415	99.0	113.3
	$B_{1,4}$	91.4	190.8	0.769	1.870	1.861	1.411	102.4	107.3
8	$^4C_1$	172.1	103.5	0.640	1.859	1.846	1.411	99.9	108.2
	$^1C_4$	5.2	299.2	0.629	1.854	1.855	1.417	99.9	113.6
	^2S_S	82.9	267.8	0.888	1.857	1.851	1.415	98.2	112.6

[a]Ring conformation.

gas phase, without noticeable differences between the two anomers. The δ_{C5} chemical shifts were similar for α- and β- anomers in the gas phase and in solution. However, the δ_{C1} results yielded distinct values.

Experimental analysis of the vicinal $^3J_{H,H}$ coupling constants usually gives key structural information for these compounds. The calculated $^3J_{H,H}$ average values by the Haasnoot-Leeuw-Altona empirical equation and by the SSCC were compared with the experimental ones. The $^3J_{H,H}$ values of the Haasnoot-Leeuw-Altona empirical equation accurately fit the experimental data, the largest errors being about 0.5 Hz for $J_{2,3}$ and $J_{5,6}$. These deviations can be considered very small, regarding the uncertainty in the experimental data (about 0.4 and 0.1 Hz, respectively). Also, it can be observed that the $^3J_{H,H}$ values show an indirect dependence with the OH orientations. Therefore, the average $^3J_{H,H}$ values depend not only on the ring form, but also on the energetic order of the different rotamers. According to these ideas, the computations in solution improved for both α- and β-anomers, because of the better distribution of rotamers.

For **3** and **4**, the ^{13}C results of the anomeric carbon are not as good as for **1** and **2**, although there is an improvement for the rest of the carbon atoms. The results of ^1H agree with the experimental data, but, as opposed to the calculated ^1H NMR data of **1** and **2**, the gas-phase results yielded better agreement than in

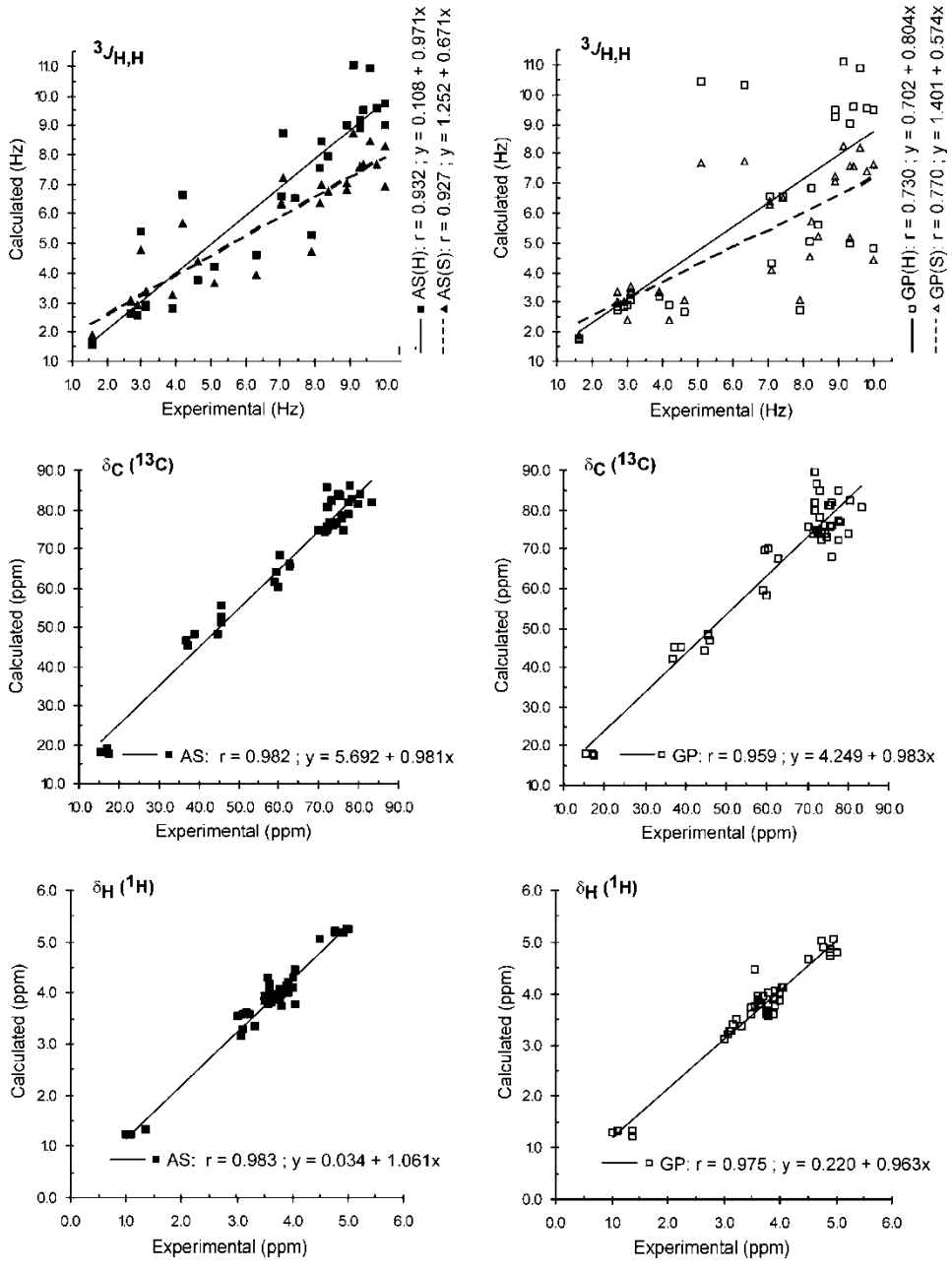

Figure 9: Calculated vs. experimental ^{1}H, ^{13}C, and $^3J_{H,H}$ data for compounds **1**–**8** together with the corresponding regression lines. AS, calculations in solution; GP, gas phase; H, calculations of $^3J_{H,H}$ coupling constants with the empirical Haasnoot-Leeuw-Altona equation, S, $^3J_{H,H}$ obtained with the SSCC method. References to the experimental data are tabulated in Table 7.

Table 5: Calculated ^{1}H NMR (GIAO method) and $^{3}J_{H,H}$ (Haasnoot equation) for **1**–**8** at the B3LYP/6–31+G* theoretical level in solution. Values corresponding to the first rotamers of each main conformation.

				δ_H (ppm)									$^{3}J_{H,H}$ (Hz)						
	Cf[a]	**CDA**[b]	**BPR**[c]	**H1**	**H2**	**H3**	**H4**	**H5**	**H6**	**H6′**	**H6″**	**H_{OMe}**	$J_{1,2}$	$J_{2,3}$	$J_{3,4}$	$J_{4,5}$	$J_{5,6'}$	$J_{5,6''}$	$J_{5,6}$[d]
1	$^{1}C_4$	t g− t t	32.7	5.2	4.1	4.0	4.4	3.8	1.3				2.9	9.8	2.7	1.7			6.6
			Exptl[e]	4.9	3.9	3.8	4.0	3.5	1.0				3.1	10.0	2.7	1.6			7.0–7.1
2	$^{1}C_4$	g+ t t t	25.1	5.0	4.0	3.7	4.3	3.6	1.3				9.1	9.7	2.5	1.6			6.6
			Exptl[f]	4.5	3.5	3.1	3.6	3.0	1.1				8.9	9.6–10.0	2.9	1.6			7.0–7.1
3	$^{4}C_1$	t g+ t t g − g −	9.2	5.3	3.8	3.9	4.1	3.4		3.6	4.6		3.0	9.5	9.1	11.1	2.0	2.1	
			Exptl[g]	5.0	3.8	3.7	3.6	3.2		3.9	3.9		3.1	9.4	8.9	9.1	3.0	5.1	
4	$^{4}C_1$	t t g− t g + g +	6.9	5.1	4.5	3.9	3.9	3.7		4.6	3.5		2.7	2.5	9.3	11.0	3.7	11.5	
			Exptl[h]	4.8	4.1	3.7	3.8	3.2		3.9	3.8		3.9	2.7	9.3	9.6	4.2	6.3	
5	$^{4}C_1$	t t t t g − g +	42.4	5.2	3.8	3.7	4.3	3.3		4.0	3.7		9.0	9.3	9.2	4.6	3.0	11.1	
5	$^{1}C_4$	g− g+ t t g − g +	0.4	5.2	4.3	4.4	4.4	4.0		3.9	4.1		2.8	3.6	3.8	1.7	2.7	10.9	
5	$^{2}S_S$	t t t t tg −	0.3	5.2	4.0	3.9	4.3	3.9		4.0	3.5		6.7	10.2	5.8	4.6	11.7	4.6	
			Avrg[i]	5.2	3.8	3.7	4.3	3.3		4.0	3.7		9.0	9.2	9.1	4.6	3.0	11.0	
			Exptl[f]	5.0	3.6	4.0	3.6	3.1		3.9	3.8		7.1	10.0	9.3				
6	$^{4}C_1$	t t t t	33.7	5.3	3.8	3.8	4.3	3.2	1.3				9.0	9.2	9.2	4.4			6.5
6	$^{1}C_4$	g− g+ t t	1.3	5.1	4.2	4.4	4.4	3.9	1.3				2.8	3.6	3.8	1.6			6.6
6	$^{2}S_S$	t t t g +	0.6	5.1	4.1	3.7	3.9	3.8	1.2				7.0	10.1	5.1	3.7			6.6

			Avrg[i]	5.3	3.9	3.8	4.3	3.2	1.3				8.7	9.1	9.0	4.3			6.5
			Exptl[f]	4.9	3.53–3.60	3.53–3.60	3.87–3.95	3.06–3.11	1.4				8.2						7.4
7	$^4C_1$	t t t t		37.6	5.2	4.0	3.5	4.3	3.4		4.4	3.7	3.7	9.2	9.6	9.2	5.1	10.9	2.7	
7	$^1C_4$	t g − g − g + t		7.8	5.2	4.4	3.9	4.7	3.7		3.9	3.6	3.5	2.9	3.4	3.8	1.5	11.2	3.3	
7	$B_{1,4}$	t t tg +		0.9	5.8	4.1	3.6	4.6	3.7		3.8	4.0	3.6	9.1	3.7	2.2	1.7	1.8	2.3	
		t t t g − g + g −																		
			Avrg[i]	5.2	4.0	3.6	4.4	3.5			4.3	3.7	3.7	8.1	8.5	8.2	4.5	10.8	2.8	
			Exptl[f]	4.8										7.9						
8	$^4C_1$	g − t t t		30.4	5.1	3.8	3.2	4.0	3.2	1.4			3.7	8.9	9.3	9.3	4.4			6.5
8	$^1C_4$	g − g + t t		3.8	5.1	4.4	3.8	4.3	3.8	1.4			3.5	2.8	3.5	3.7	1.6			6.6
8	^2S_S	t g − g + g +		1.7	5.1	4.0	3.2	4.0	3.8	1.4			3.7	6.4	10.1	5.0	3.5			6.6
			Avrg[i]	5.1	3.8	3.3	4.1	3.3	1.4				3.7	8.1	8.7	8.5	4.1			6.6
			Exptl[f]	4.9	3.7	3.3	4.0		1.4					8.0–8.3	8.4	8.2–8.6	4.6			

[a]Ring conformation.
[b]Classification by dihedral angles (see text); the OH groups are numbered according to the ring carbons (see Fig. 2).
[c]Boltzman population rate.
[d]From the equivalent H(6) methyl protons.
[e]From ref. (33).
[f]From ref. (33).
[g]From ref. (59).
[h]From ref. (24).
[i]Averaged values of the three rotamers according to their populations rate.

solution. As a general trend, the $^3J_{H,H}$ data calculated in solution, compared with those in the gas phase, clearly agreed better with the experimental data, not only for **3** and **4**, but also for all the compounds studied. Particularly for $J_{5,6'}$, the results failed in the gas phase, presumably due to the overestimation of the OH(6)···OH(4) interaction in the first rotamer for **3** and **4**.

For L-ido derivatives (**5**–**8**), although not all the signals are assigned experimentally, the $J_{1,2}$ anomeric couplings, which give the most relevant structural information ($^1C_4$ vs. $^4C_1$ or α vs. β), agreed well with the available experimental data.[54] For both deoxy and non deoxy derivatives, only the data from calculations in solution fit correctly. For deoxy compounds, the disagreement of the gas phase results was caused by the aforementioned overestimation of the $^1C_4$ ring form, while in the non deoxy compounds, the disagreement is much more evidenced, because the same overestimation leads to the inversion of the chair ring-form conformational preference. With respect to the chemical shifts of **5**–**8**, even though there is a lack of experimental data for **7**, the main tendencies for the δ_C and δ_H shifts are similar to those found for **3** and **4**.

For all compounds, the SSCC method failed to reproduce the high values of $^3J_{H,H}$, giving lower values than those of the Haasnoot-Leeuw-Altona empirical equation, with the deviation of SSCC data from the experiment being much larger.

Figure 9 shows the theoretical data of ^1H, ^{13}C, and $^3J_{H,H}$ correlated with the experimental data when available. As reflected in Figure 9, a better agreement was consistently found for calculations in solution, with good regression values *r*. Moreover, in the case of $^3J_{H,H}$, the Haasnoot-Leew-Altona empirical equation in solution gave the best agreement with the experiment.

Figure 10 displays the correlation of the experimental $^3J_{H,H}$ couplings with the calculated Haasnoot and SSCC values, respectively. In order to visualize the different degree of correlation, the graphics have been arranged in three different series. The first series includes compounds **1** and **2** and presents a high degree of correlation for both theoretical methods.

On the other hand, for the remaining series the scattering is more pronounced. In the second series, which includes compounds **3** and **4**, the scattering is caused mainly by the $J_{5,6'}$ and $J_{5,6''}$ couplings, which correspond to the free rotation of the CH_2OH group. In fact, for **3**, the theoretical values are improved after considering the averaged values of the seven first rotamers. All of these rotamers present the [t g+ t t] classification of dihedral angles for the ring carbon atoms, and differ only in the classification of CH_2OH group rotation. Furthermore $J_{5,6'}$ and $J_{5,6''}$ couplings do not contribute to the elucidation of the ring conformation ($^4C_1$ chair form).

The third series (L-ido compounds **5**–**8**) yielded the worst correlation, undoubtedly due to the $J_{1,2}$ value of **5** and **7**. For some of the compounds included in this series, there are scarce experimental data, avoiding a better correlation. Despite these difficulties, it can be stated that the conformational

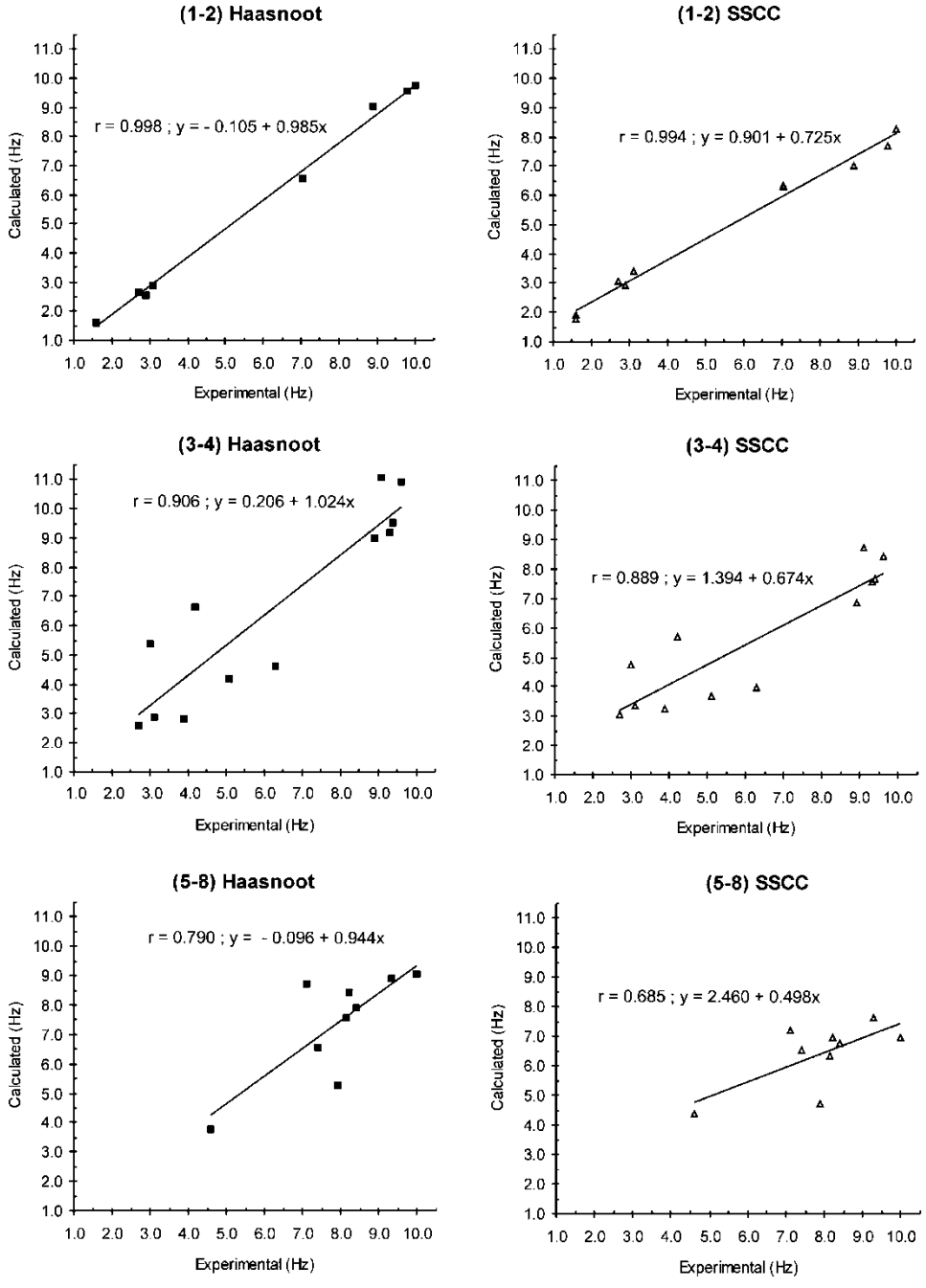

Figure 10: Calculated (Haasnoot-Leeuw-Altona equation, and SSCC method) vs. experimental $^{3}J_{H,H}$ coupling constants for compounds **1**–**8** in solution together with the corresponding regression lines. References to the experimental data are tabulated in Table 7.

Table 6: Comparative Results[a] between B3LYP/6–31+G* and MP2/6–311++G** calculations of selected structures for **2** in the gas phase, and for **6** and **8** in aqueous solution.

			B3LYP/6-31+G*		MP2/6-311++G**	
	Cf[b]	**CDA**[c]	**ΔE**[d]	**BPR**[e]	**ΔE**[d]	**BPR**[e]
2	$^1C_4$	g− g+ g+ g +	0.00 (0.00)	95.8 (82.0)	0.00	98.0
	$^1C_4$	t g+ g+ g +	2.05 (1.94)	3.0 (3.1)	2.32	1.9
	$^4C_1$	g+ g− g− t	3.11 (1.66)	0.5 (4.9)	5.06	0.0
	$^4C_1$	g+ g− g− g −	3.14 (1.58)	0.5 (5.7)	4.73	0.0
	$^4C1$	g+ g− t g +	3.79 (2.53)	0.2 (1.2)	5.79	0.0
	$^5S_1$	g+ g− g+ t	4.22 (1.94)	0.1 (3.1)	7.82	0.0
6	$^4C_1$	t t t t	0.00	94.7	0.00	95.2
	$^1C_4$	g− g+ t t	1.94	3.6	1.93	3.7
	^2S_S	t t t g +	2.36	1.8	2.65	1.1
8	$^4C_1$	g− t t t	0.00	84.7	0.00	65.9
	$^1C_4$	g− g+ t t	1.22	10.7	0.48	29.3
	^2S_S	t g− g+ g +	1.72	4.6	1.55	4.8

[a]In parenthesis data calculated at the B3LYP/6-31G* level.
[b]Ring conformation.
[c]Classification by dihedral angles.
[d]Relative energy in kcal/mol.
[e]Boltzman population rate.

order is $^4C_1 > {}^1C_4 > {}^2S_S$ ($B_{1,4}$ in case of **7**) for all the L-ido compounds here studied. Although in some particular cases, the comparison of the anomeric $J_{1,2}$ coupling constant (only experimentally available for **6** and **7**) could raise doubts about whether the $^4C_1$ or ^2S_S are the main ring form, the $J_{3,4}$ data clearly support the $^4C_1$ form. This is additionally supported by calculations at a higher level of theory (MP2/6–311++G**) for some of these structures, yielding the same conformational preference (see Table 6).

Besides, Table 5 presents the ^1H chemical shifts and $^3J_{H,H}$ coupling constants, arranged by conformation (the most populated). This table allows a direct comparison of the spectroscopic data for the possible conformation of

Table 7: List of references corresponding to the sources of the NMR experimental data.

Compound	**δ_C (^{13}C)**	**δ_H (^1H)**	**$^3J_{H,H}$**
1	33	33	33
2	—	33	33
3	59	59	59
4	23, 24	24	24
5–8	33	33	33

each compound. Compounds **1**–**4** yielded only one main $^1C_4$ or $^4C_1$ conformation, in agreement with the experimental coupling constants. For L-ido compounds **5**–**8**, where the computed data showed three main conformations, the agreement between the averaged computed and experimental coupling constants was very good. Generally, good results are obtained with the exception of $J_{5,6'}$ and $J_{5,6'}$ of **3** and **4**, as it is explained above.

CONCLUSIONS

A conformational analysis of different 5-thio-pyranose derivatives was performed by MM and DFT methods in the gas phase and in solution with the PCM. In contrast with their natural homolog, the inclusion of diffuse functions was necessary for a correct reproduction of the rotamer population, yielding the calculations without diffuse-function erroneous results on the relative energy orders, overestimating the stabilizing OH(n)···S_{ring} interactions.

The calculations in solution (PCM-B3LYP/6–31 + G*) accurately reproduced the reported experimental data, while gas-phase calculations failed. Gas-phase results showed different relative rotamer-energy orders and conformational preferences than in solution. In particular, for L-ido derivatives (**5**–**8**), the calculations in the gas phase did not match the experimental conformational preference, even inverting the order of the $^1C_4$ and $^4C_1$ chair forms for nondeoxy derivatives. Therefore, the gas-phase calculations were not suitable to describe the preferences in solution.

The OH(6) was revealed as a key element in determining the conformational order because of the additional and more stabilizing nonadjacent intramolecular interactions. Additionally, for **7**, the presence of a methyl group at C_3 caused the $B_{1,4}$ boat conformation to be preferred over the ^2S_S skew-boat as the third ring form.

The main ring form for **1** and **2** in the gas phase presented a maximal number of OH···O intramolecular interactions. These interactions were arranged as intramolecular anticlockwise (or clockwise) unidirectional chains of the hydroxyl groups, similar to their natural counterparts. Moreover, when these interactions were directed at one oxygen (bidirectional chains), the resulting conformations became less stable. It was found that OH(n)···S_{ring} interactions were a source of additional stabilization. However, the calculations in solution indicated that 5-thio-pyranose derivatives tend to break their intramolecular OH···O interactions, favoring the interaction of the OH groups with the solvent molecules. Also, the conformational analysis revealed that, after inclusion of the solvent in the calculations, the different rotamers were energetically ordered, according to the exo-anomeric effect.

From the conformation analysis, it was found that the "hockey-stick" effect is reproduced only theoretically in solution, where conformations compatible with this effect appear stabilized with OH···O interactions. Therefore, the

validity of the "hockey-stick" effect is questioned for the gas phase, and further investigation is needed.

The exo-anomeric effect is correctly reproduced only with the B3LYP/6–31 + G* method including the PCM solvation method. The bond distances related to this effect are reproduced, as well as the rotamer-energy order caused by the exo-anomeric effect. This highlights the necessity of considering the solvent for the study of these and other carbohydrates.

The GIAO-calculated NMR ^{1}H chemical shifts accurately reproduced the experimental trends for the thiosugars studied. However, ^{13}C chemical shifts were less accurate. The $^{3}J_{H,H}$ coupling constants calculated in solution with the Haasnoot-Leeuw-Altona empirical equation also matched the experimental data. However, the $^{3}J_{H,H}$ calculations with SSCC were in disagreement for high coupling-constant values, these being lower than those obtained with the Haasnoot-Leeuw-Altona equation. It is worth mentioning that, for an accurate reproduction of spectroscopic properties, it is necessary to take into account the Boltzman population rates.

SUPPLEMENTARY DATA

Pdb files of the rotamers for compounds **1**–**8**, computed at the PCM-B3LYP/6–31+G* theoretical level, are available at www.ugr.es/local/gmdm/supinf/thio1.htm.

ACKNOWLEDGMENTS

This work was supported from the Junta de Andalucía (FQM-174). Computing time has been provided by the University of Granada (Spain). We are grateful to Professor F. Santoyo and Dr. S. Melchor for invaluable advice and comments on the manuscript, and to Professor J. Isac for help on NMR discussion. Mr David Nesbitt reviewed the original English manuscript.

REFERENCES

[1] Ganem, B. Inhibitors of carbohydrate-processing enzymes: design and synthesis of sugar-shaped heterocycles. Acc. Chem. Res. **1996**, *29*, 340–347.

[2] Yuasa, H.; Saotome, C.; Kanie, O. Design syntheses of inhibitors of glycoenzymes. Trends Glycosci. Glyc. **2002**, *14*, 231–251.

[3] Simanek, E.E.; McGarvey, G.J.; Jablonowski, J.A.; Wong, C.H. Selectin-carbohydrate interactions: from natural ligands to designed mimics. Chem. Rev. **1998**, *98*, 833–862.

[4] Sears, P.; Wong, C.H. Carbohydrate mimetics: a new strategy for tackling the problem of carbohydrate-mediated biological recognition. Angew. Chem. Int. Ed. **1999**, *38*, 2300–2324.

[5] Yuasa, H.; Hashimoto, H. Recent advances in the development of unnatural oligosaccharides. Conformation and bioactivity. Trends Glycosci. Glyc. **2001**, *13*, 31–55.

[6] Atsushi, K.; Noriko, K.; Erika, K.; Isao, A.; Kyoko, I.; Liang, Y.; Tadashi, O.; Yasunori, B.; Hidekazu, O.; Hiroki, T.; Naoki, A. Biological properties of D- and L-1-deoxyazasugars. J. Med. Chem. **2005**, *48*, 2036–2044.

[7] Yuasa, H.; Hashimoto, H. Replacing the ring oxygen of carbohydrates with sulfur: its biological and chemical consequences. Rev. Heteroatom. Chem. **1999**, *19*, 35–65.

[8] Fernández-Bolaños, J.G.; Al-Masoudi, N.A.L.; Maya, I. Sugar derivatives having sulfur in the ring. Adv. Carbohydr. Chem. Biochem. **2001**, *57*, 21–98.

[9] Robina, I.; Vogel, P.; Witczak, Z.J. Synthesis and biological properties of monothiosaccharides. Curr. Org. Chem. **2001**, *5*, 1177–1214.

[10] Paulsen, H.; Todt, K. Cyclic monosaccharides having nitrogen or sulfur in the ring. Adv. Carbohydr. Chem. **1968**, *23*, 115–232.

[11] Robina, I.; Vogel, P. The synthesis of disaccharides, oligosaccharides and analogues containing thiosugars. Curr. Org. Chem. **2002**, *6*, 471–491.

[12] Tsuruta, O.; Yuasa, H.; Hashimoto, H.; Sujino, K.; Otter, A.; Li, H.; Palcic, M.M. Synthesis of GDP-5-thiosugars and their use as glycosyl donor substrates for glycosyltransferases. J. Org. Chem. **2003**, *68*, 6400–6406.

[13] Schwarz, J.C.P.; Yule, K.C. D-xylothiapyranose - a sugar with sulphur in ring. Proc. Chem. Soc. **1961**, 417.

[14] Adley, T.J.; Owen, L.N. Thio-sugars with sulphur in ring. Proc. Chem. Soc. **1961**, 418.

[15] Whistler, R.L.; Nayak, U.G. Improved syntheses of 5-thio-D-glucose. J. Org. Chem. **1969**, *34*, 97–100.

[16] Hellman, B.; Lemmark, Å.; Sehlin, J.; Taljedal, I.B.; Whistler, R.L. Accumulation of collagen in the uterus of the immature rat administered estradiol-17$^{\beta}$. Biochem. Pharmacol. **1973**, *22*, 29–35.

[17] Kim, J.H.; Kim, S.H.; Han, E.W.; Song, C.W. 5-Thio-D-glucose selectivity potentiates hyperthermia killing of hypoxic tumor-cells. Science **1978**, *200*, 206–207.

[18] Inamori, Y.; Muro, C.; Toyoda, M.; Kato, Y.; Tsujibo, H. Inhibitory activity of 5-thio-D-glucose on plant-growth. Biosci. Biotech. Biochem. **1994**, *58*, 1877–1878.

[19] Izumi, M.; Tsuruta, O.; Hashimoto, H. A facile synthesis of 5-thio-L-fucose and 5-thio-D-arabinose from D-arabinose. Carbohydr. Res. **1996**, *280*, 287–302.

[20] Hashimoto, H.; Kawanishi, M.; Yuasa, H. Novel conversion of aldopyranosides into 5-thioaldopyranosides via acyclic monthioacetals with inversion and retention of configuration at C-5. Carbohydr. Res. **1996**, *282*, 207–221.

[21] Le Merrer, Y.; Fuzier, M.; Dosbaa, I.; Foglietti, M.J.; Depezay, J.C. Synthesis of thiosugars as weak inhibitors of glycosidases. Tetrahedron **1997**, *53*, 16731–16746.

[22] Cubero, I.I.; López-Espinosa, M.T.P.; Richardson, A.C.; Ortega, M.D.S. Enantiospecific synthesis of 1-deoxythiomannojirimycin from a derivative of D-glucose. Carbohydr. Res. **1993**, *242*, 109–118.

[23] Yuasa, H.; Izukawa, Y.; Hashimoto, H. Synthesis of 5-thio-D-mannose. J. Carbohydr. Chem. **1989**, *8*, 753–763.

[24] Capon, R.J.; MacLeod, J.K. 5-Thio-D-mannose from the marine sponge Clathria Pyramida (Lendenfeld). The first example of a naturally occurring 5-thiosugar. J. Chem. Soc., Chem. Commun. **1987**, 1200–1201.

[25] Yuasa, H.; Takada, J.; Hashimoto, H. Synthesis of salacinol. Tetrahedron Lett. **2000**, *41*, 6615–6618.

[26] Imberty, A.; Pérez, S. Structure, conformation, and dynamics of bioactive oligosaccharides: theoretical approaches and experimental validations. Carbohydr. Res. **2000**, *100*, 4567–4588.

[27] Panday, N.; Meyyappan, M.; Vasella, A. A comparison of glucose- and glucosamine-related inhibitors: probing the interaction of the 2-hydroxy group with retaining β-glucosidases. Helv. Chim. Acta **2000**, *83*, 513–538.

[28] Wormald, M.R.; Petrescu, A.J.; Pao, Y.; Glithero, A.; Elliott, T.; Dwek, R.A. Conformational studies of oligosaccharides and glycopeptides: complementarity of NMR, X-ray crystallography, and molecular modelling. Chem. Rev. **2002**, *102*, 371–386.

[29] The anomeric effect has been explained by decreasing the dipole-dipole repulsion between C-O bonds in the axial anomer (Edward, J.T. Stability of glycosides to acid hydrolysis - a conformational analysis. Chem. Ind. (London) **1955**, *36*, 1102–1104. Anderson, C.B.; Sepp, D.T Conformation and the anomeric effect in 2-oxy-substituted tetrahydropyrans. Tetrahedron **1968**, *24*, 1707–1716) and/or from greater hyperconjugative stabilization of pyranose oxygen lone-pair density, when delocalized into the empty axial σ^*CO orbital (Romers, C.; Altona, C.; Buys, H.R.; Havinga E. In *Topics in Stereochemistry*; Eliel, E.L., Allinger, N.L., Eds.; Wiley: New York, **1969**; Vol. 4, 39).

[30] Woods, R.J.; Smith, J.V.H.; Szarek, W.A.; Farazdel, A. *Ab initio* LCAO-MO calculations on α-D-glucopyranose, β-D-fructopyranose, and their thiopyranoid-ring analogues. Application to a theory of sweetness. J. Chem. Soc., Chem. Commun. **1987**, 937–939.

[31] Kavlekar, L.M.; Kuntz, D.A.; Wen, X.; Jonshton, B.D.; Svensson, B.; Rose, D.R.; Mario Pinto, B. 5-Thio-D-glycopyranosylamines and their amidinium salts as potential transition-state mimics of glycosyl hydrolases: synthesis, enzyme inhibitory activities, X-ray crystallography, and molecular modeling. Tetrahedron: Asymm. **2005**, *16*, 1035–1046.

[32] Wong, C.H. Mimics of complex carbohydrates recognized by receptors. Acc. Chem. Res. **1999**, *32*, 376–385.

[33] Calvo-Flores, F.G.; García-Mendoza, P.; Hernández-Mateo, F.; Isac-García, J.; Santoyo-González, F. Applications of cyclic sulfates of vic-diols: synthesis of episulfides, olefins, and thio sugars. J. Org. Chem. **1997**, *62*, 3944–3961.

[34] Csonka, G.I.; Élías, K.; Csizmadia, I.G. *Ab initio* and density functional study of the conformational space of $^1C_4$ α-L-fucose. J. Comput. Chem. **1996**, *18*, 330–342.

[35] Csonka, G.I.; Éliás, K.; Csizmadia, I.G. Relative stability of $^1C_4$ and $^4C_1$ chair forms of β-D-glucose: a density functional study. Chem. Phys. Lett. **1996**, *257*, 49–60.

[36] Lemieux, R.U. How water provides the impetus for molecular recognition in aqueous solution. Acc. Chem. Res. **1996**, *29*, 373–380.

[37] Tomasi, J.; Persico, M. Molecular interactions in solution: an overview of methods based on continuous distributions of the solvent. Chem. Rev. **1994**, *94*, 2027–2094.

[38] Cramer, C.J.; Truhlar, D.G. Implicit solvation models: equilibria, structure, spectra, and dynamics. Chem. Rev. **1999**, *99*, 2161–2200.

[39] Duus, J.Ø.; Gotfredsen, C.H.; Bock, K. Carbohydrate structural determination by NMR spectroscopy: modern methods and limitations. Chem. Rev. **2000**, *100*, 4589–4614.

[40] Herfurth, L.; Weimar, T.; Peters, T. Application of 3D-TOCSY-trNOESY for the assignment of bioactive ligands from mixtures. Angew. Chem. Int. Ed. **2000**, *39*, 2097–2099.

[41] Helgaker, T.; Watson, M.; Handy, N.C. Analytical calculation of nuclear magnetic resonance indirect spin-spin coupling constants at the generalized gradient approximation and hybrid levels of density-functional theory. J. Chem. Phys. **2000**, *113*, 9402–9409.

[42] Sychrovský, V.; Gräfenstein, J.; Cremer, D. Nuclear magnetic resonance spin-spin coupling constants from coupled perturbed density functional theory. J. Chem. Phys. **2000**, *113*, 3530–3547.

[43] Haassnoot, C.A.G.; De-Leeuw, F.A.A.M.; Altona, C. The relationship between proton-proton NMR coupling constants and substituent electronegativities-I (an empirical generalization of the Karplus equation). Tetrahedron **1980**, *36*, 2783–2792.

[44] A modification of the Allinger's MM2(77) (Allinger, N.L. Conformational analysis. 130. MM2. A hydrocarbon force field utilizing V_1 and V_2 torsional terms. J. Am. Chem. Soc. **1977**, *99*, 8127–8134) and MMP1 programs (Allinger, N.L.; Sprague, J.T. Calculation of the structures of hydrocarbons containing delocalized electronic systems by the molecular mechanics method. J. Am. Chem. Soc. **1973**, *95*, 3893–3907) by Gajewski and Gilbert implemented in the PCMODEL program (available on Serena Software, PO Box, 3076, Bloomington, IN 47402–3076, USA).

[45] We used the Cremer and Pople puckering coordinates algorithm (see Cremer, D.; Pople, J.A A general definition of ring puckering coordinates. J. Am. Chem. Soc. **1975**, *97*, 1354–1358) to classify the ring form.

[46] Frisch, M.J.; Trucks, G.W.; Schlegel, H.B.; Scuseria, G.E.; Robb, M.A.; Cheeseman, J.R.; Montgomery, J.A., Jr.; Vreven, T.; Kudin, K.N.; Burant, J.C.; Millam, J.M.; Iyengar, S.S.; Tomasi, J.; Barone, V.; Mennucci, B.; Cossi, M.; Scalmani, G.; Rega, N.; Petersson, G.A.; Nakatsuji, H.; Hada, M.; Ehara, M.; Toyota, K.; Fukuda, R.; Hasegawa, J.; Ishida, M.; Nakajima, T.; Honda, Y.; Kitao, O.; Nakai, H.; Klene, M.; Li, X.; Knox, J.E.; Hratchian, H.P.; Cross, J.B.; Adamo, C.; Jaramillo, J.; Gomperts, R.; Stratmann, R.E.; Yazyev, O.; Austin, A.J.; Cammi, R.; Pomelli, C.; Ochterski, J.W.; Ayala, P.Y.; Morokuma, K.; Voth, G.A.; Salvador, P.; Dannenberg, J.J.; Zakrzewski, V.G.; Dapprich, S.; Daniels, A.D.; Strain, M.C.; Farkas, O.; Malick, D.K.; Rabuck, A.D.; Raghavachari, K.; Foresman, J.B.; Ortiz, J.V.; Cui, Q.; Baboul, A.G.; Clifford, S.; Cioslowski, J.; Stefanov, B.B.; Liu, G.; Liashenko, A.; Piskorz, P.; Komaromi, I.; Martin, R.L.; Fox, D.J.; Keith, T.; Al-Laham, M.A.; Peng, C.Y.; Nanayakkara, A.; Challacombe, M.; Gill, P.M.W.; Johnson, B.; Chen, W.; Wong, M.W.; Gonzalez, C. *Gaussian 03, Revision B.05*; Gaussian, Inc: Pittsburgh, PA, 2003.

[47] Cramer, C.J.; Truhlar, D.G. Quantum chemical conformational analysis of glucose in aqueous solution. J. Am. Chem. Soc. **1993**, *115*, 5745–5753.

[48] Stewart, J.J.P. Optimization of parameters for semiempirical methods I. Method. J. Comput. Chem. **1989**, *10*, 209–220.

[49] Onsager, L. Electric moments of molecules in liquids. J. Am. Chem. Soc. **1936**, *58*, 1486–1493.

[50] Wolinski, K.; Hinton, J.F.; Pulay, P. Efficient implementation of the gauge-independent atomic orbital method for NMR chemical shift calculations. J. Am. Chem. Soc. **1990**, *112*, 8251–8260.

[51] Csonka, G.I.; Élías, K.; Kolossváry, I.; Sosa, C.P.; Csizmadia, I.G. Theoretical study of alternative ring forms of α-L-fucopyranose. J. Phys. Chem. A **1998**, *102*, 1219–1229.

[52] The exo-anomeric effect is commonly defined as the stabilization favored when the substituent of the anomeric OR (R=H in this case) is gauche with respect to the O/S_{ring} (Kirby, A.J. *The Anomeric Effect and Related Stereoelectronic Effects at Oxygen*; Springer-Verlag: Berlin Heidelber NewYork, **1983**), For $^1C_4$ ring form of **1** this situation is done for *1t* orientation. The *1 g+*, one is non-exo, and the *1 g-*, although it is exo, shows 1-3-diaxial-type repulsion with axial hydrogen on C3 and C5.

[53] Mehta, S.; Jordan, K.L.; Weimar, T.; Kreis, U.C.; Batchelor, R.J.; Einstein, F.W.B.; Mario Pinto, B. Synthesis of sulfur analogues of methyl and allyl kojibiosides and methyl isomaltoside and conformational analysis of the kojibiosides. Tetrahedron: Asymm. **1994**, *5*, 2367–2396.

[54] Hughes, N.A.; Munkombwe, N.M.; Todhunter, N.D. Synthesis of derivatives of 5-thio-L-idose. Carbohydr. Res. **1991**, *216*, 119–139.

[55] López de la Paz, M.; Ellis, G.; Pérez, M.; Perkins, J.; Jiménez-Barbero, J.; Vicent, C. Carbohydrate hydrogen-bonding cooperativity - intramolecular hydrogen bonds and their cooperative effect on intermolecular processes - binding to a hydrogen-bond acceptor molecule. Eur. J. Org. Chem. **2002**, 840–855.

[56] Longchambon, F.; Ohannessian, J.; Avenel, D.; Neuman, A. Structure cristalline du β-D-galactose et de l'α-L-Fucose. Acta Cryst. **1975**, *31*, 2623–2627.

[57] Cramer, C.J.; Truhlar, D.G.; French, A.D. Exo-anomeric effects on energies and geometries of different conformations of glucose and related systems in the gas phase and aqueous solution. Carbohydr. Res. **1997**, *298*, 1–14.

[58] Izumi, K. NMR spectra of some monosaccharides of galactopyranose series in deuterium oxide. Agr. Biol. Chem. **1971**, *35*, 1816–1818.

[59] Lambert, J.B.; Wharry, S.M. Conformational analysis of 5-thio-D-glucose. J. Org. Chem. **1981**, *46*, 3193–3196.